HU ISSN 1785-6892 in print
HU ISSN 2064-7522 online

DESIGN OF MACHINES AND STRUCTURES

A Publication of the University of Miskolc

Volume 10, Number 1

Miskolc University Press
2020

EDITORIAL BOARD

CONTENTS

Design of Machines and Structures, Vol. 10, No. 1 (2020), pp. 5–12.
Doi: 10.32972/dms.2020.001

EFFECT OF THE WELDING PARAMETERS ON RESIDUAL STRESSES IN PIPE WELD USING NUMERICAL SIMULATION

MAHMOOD ALHAFADHI[1]–GYÖRGY KRÁLLICS[2]

University of Miskolc, Faculty of Material Science and Engineering,
3515, Miskolc-Egyetemváros
mahmoodhs199@gmail.com

Abstract: The objective of this article is to predict the residual welding stress in a dissimilar pipe weld. The 2D model, instead of 3D was used to reduce the time and cost of the numerical calculation. The 2D numerical simulation MSC MARC code is used to predict the residual stress developed during pipe welding. The present model was validated using hardness measurement. Good agreement was found between the measurement and numerical simulation results. The effects of welding parameters on residual stress field on the outer and inner surface were assessed. The effect of welding parameter (welding current) is examined. The axial and hoop residual stresses in dissimilar pipe joints of different thickness for pipe weld were simulated in outer and inner surfaces. When the other parameters remain fixed, and the current has great effect on the weld shape and size, and then affects the residual stress level significantly.

Keywords: *Numerical Simulation, Welding Pipe, Residual stress.*

1. INTRODUCTION

Welding is a reliable and efficient metal joining process between two parts of dissimilar pipes. Arc welding joints are more extensively used in the fabrication industry, oil and gas pipeline, offshore structures, and pressure vessels. Welding residual stresses are caused by differential thermal expansion and contraction of the weld metal and dissimilar base metal. Further, these residual stresses can be of either tensile type or the compressive type, depending upon the location of the non-uniform volumetric change. Numerical simulation is used to predict residual stresses due to the complexity of the shape structure. Nowadays, it is possible to use numerical simulation techniques to predict the residual stresses in welded structures and it can be employed to simulate welding temperature field and welding deformation. [1–7]. In order to reduce the computational time and cost, most of the researchers choose the 2D model. Brickstad and Josefon [8] employed 2D model to simulate welding of stainless steel pipe in thermo-mechanical finite element analysis. Dean Deng et al. [9] presented a 2D FE model for simulating residual stresses during multipass welding of a pipe. The distribution of residual stress in welded pipe structures depends on several factors such as structural dimensions material properties, and heat input, etc. Siddique M. et al. [10] analysed the residual stress fields in circum-

ferentially arc welded and studied the effect of two basic welding parameters including welding current and speed. However, there are minimal studies on effects of welding parameters on residual stresses in dissimilar welded pipe joints. In this study, the prediction of residual stresses in a dissimilar pipe weld joint made of E355K2 and P460NH_1 is studied by using 2D finite element method. This study also presents the 2D FE model of pipe joint to investigate the effect of welding current on residual stress distribution.

2. 2D AND 3D MODELLING PROCESS

A dissimilar pipe with outer diameter of 114.3 mm, with different thickness of 8 mm and 11, and a total length of 800 mm as shown in *Figure1* is considered for the analysis. The meshed model of pipe is shown in *Figure 1(b)*. The material used are, P460NH_1 steel, E355K2 steel and filler metal Böhler and its mechanical and thermal properties with varying temperature are shown in *Figure 2*.

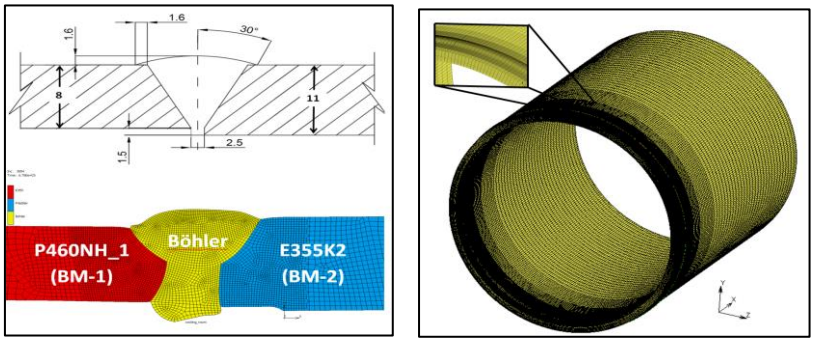

Figure 1. (a) 2D finite element model with dimension (mm)
(b) 3D finite element model of pipe

In this study, three pass welding with an inter-pass temperature of 50 °C is used. Chemical composition of the pipe used in this study is given in *Table 1*.

Table 1
Chemical composition (wt%)

Materials	C	S	P	Mn	Si	V	Cr	Cu
Base material P460NH_1	0.2	0.001	0.02	1.49	0.33	0.2	0.01	0.03
Base material E355K2	0.13	0.01	0.86	0.86	0.01	0.058	0.02	0.02
Filler metal Böhler	0.1	–	0.02	0.4	0.14	–	0.1	0.17

Thermal cycles at the weld zone of the pipe are shown in *Figure 2*. All region in and around the weld of pipe have a maximum temperature of 620 °C. It can see the sudden drop of temperature in minimum time intervals.

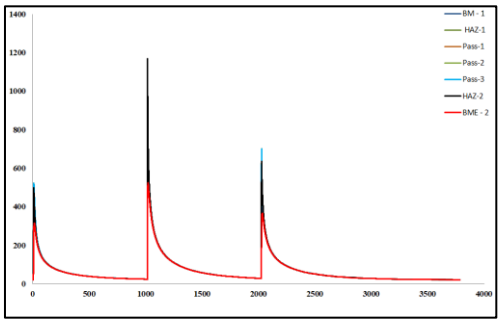

Figure 2. Thermal cycle all region in the weld

3. THERMAL AND MECHANICAL ANALYSIS

Analysis is done for a V-grooved weld since the pipe is unsymmetrical, the pipe is modeled. By using appropriate mesh optimization technique, relatively fine mesh is created in and around the weld centreline and coarse mesh is in areas away from weld line as shown in *Figure 1(a)*. Four nodes and 86,642 thermal and mechanical elements are used for the analysis. The equations are used for transient heat transfer and heat source with a double ellipsoidal distribution proposed by Goldak et al. during welding is given by [1]

$$pc\frac{\partial T}{\partial t(x,y,z,t)} = -\nabla q(x,y,z,t) + Q(x,y,z,) \tag{1}$$

$$Q(x,y,z,t) = \frac{6\sqrt{3}\, f_i \eta IV}{abc_f \pi\sqrt{\pi}} e^{-3\left(\frac{x-vt}{a}\right)^2} e^{-3\left(\frac{y}{b}\right)^2} e^{-3\left(\frac{z}{c}\right)^2} \tag{2}$$

Where p is the density of the materials, c is the specific heat capacity, q is the heat flux vector, T is the temperature, Q is the inside heat rate, x, y and z are the coordinates in the system, t is time and ∇ is the spatial gradient operator. The various weld parameters in a double ellipsoidal distribution proposed by Goldak et al. [11] *(*see *Figure 3)*. Where x, y, and z are the coordinates of the Goldak double ellipsoid model, π is the fraction of heat deposited in the weld region, the heat input rate Q = ηVI is calculated by welding operational parameters current (I), voltage (V) and η is the arc efficiency for the welding process, *v* is the speed of torch travel in mm/s, and t is the time in seconds. The factors f_f and f_r refer to the fraction of the heat deposited in the front and rear quadrant respectively, which are set up to attain the restriction $f_f + f_r = 2$. The parameters a, b and c are related to the characteristics of the welding heat source. The parameters of the heat source are chosen according to the welding conditions. The same element mesh is used in the thermal analysis and the mecha-

nical analysis. During the welding process, the solid-state phase transfor-mation occurs in the base metal and the weld metal. Therefore the total strain rate can be expressed as follows:

$$\boldsymbol{\varepsilon} = \boldsymbol{\varepsilon_e} + \boldsymbol{\varepsilon_p} + \boldsymbol{\varepsilon_{th}} \tag{3}$$

Where the elastic strain is $\boldsymbol{\varepsilon_e}$, the plastic strain $\boldsymbol{\varepsilon_p}$ and $\boldsymbol{\varepsilon_{th}}$ is the thermal strain.

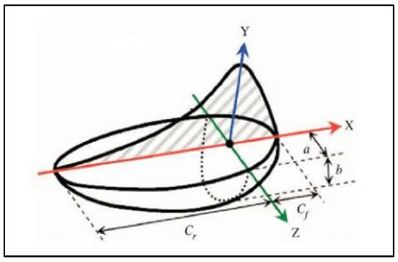

Figure 3. Double-ellipsoidal volumetric heat source model

4. VALIDATION 2D PIPE MODEL

The Cross-sectional views of the hardness test shown in *Figure 4* and the 2D model is validated using hardness measurement. The predicted simulation results are in good agreement with the measurement results, as shown in *Figure 4*.

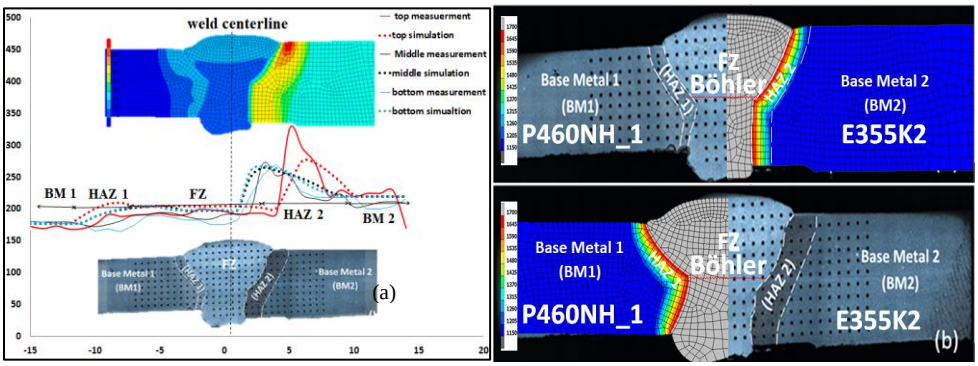

Figure 4. (a) Comparison between the predicted hardness simulation and the hardness measurement (b) Simulated temperature distributions in the cross-section

Figure 4 (b) shows the peak temperature experienced during welding enveloped over all three passes. The resulting final fusion zone is indicated by the region with the temperature above 1,650 °C. Heat affective zone (HAZ-1) and (HAZ-2) are outlined approximately by the temperature interval between about 1,000 °C and 1,600 °C

5. RESULTS AND DISCUSSION

5.1. Axial, radial and hoop residual stress on the outer and inner surface

Residual stresses predicted from 2D model simulation results on the outer and the inner surfaces, as shown in *Figure 5*. Maximum tensile axial stresses in the weld region were on the inner surface approximately 340 MPa located near HAZ-1 of the base metal (P460NH_1). Axial compressive stresses of roughly 350 MPa in the outer surface and radial stresses up to around 200 MPa was observed in the inner surface weld region. Hoop stresses up to ~ 100 MPa were found in the inner surface pipe weld and 85 in the outer surface, but it can see that the high values in the middle of weld region.

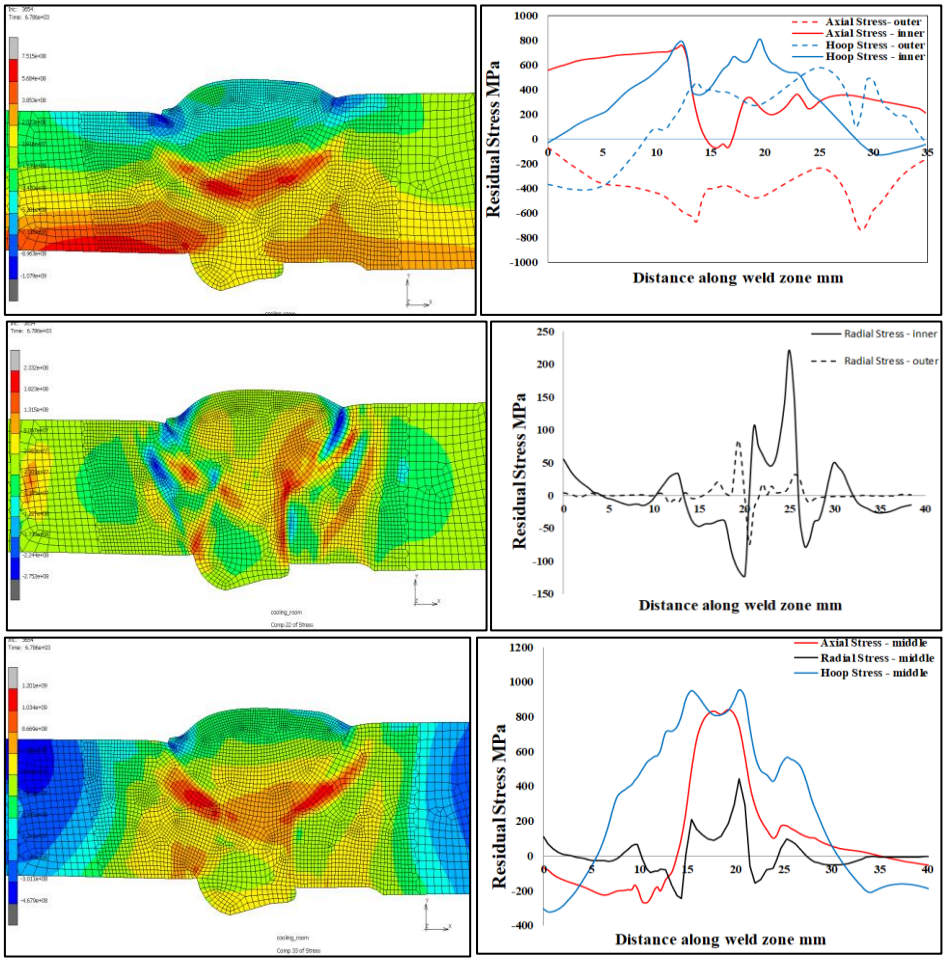

Figure 5. variation of axial, radial and hoop residual stress in the inner, outer and middle weld region

5.2. Effect of welding parameters

The residual stress calculation of weld pipe as a function of distance for current (70, 80 and 100 A) is shown in *Table 2*. From *Figure 6*, we can observe that the range of stress becomes wider with increasing welding currents. To clarify the welding current change influences on welding residual stress, Welding residual stresses at the outer and inner surfaces from the weld start point for different welding current combinations in three pass welding. Three main regions on inner weld surface (HAZ, FZ and BM) of the axial residual stress in the weld are shown in the *Figure (a)*: compressive stress (regions BM-1, BM-2, HAZ-1, HAZ-2 and FZ) and tensile stress (region FZ) in case B. It means that for welding currents (case A) with current 70 A the limit of stress are about 455 MPa in tension and 213 MPa in compression on outer and inner weld surface. But for the 100 A the maximum stress range is 800 MPa and in tension and 650 MPa in compression. The same is true for the stress plot of inner surface of pipe show in *Figure (b)*.

Table 2
Welding parameter cases and welding pool

Cases	Current (A)	Voltage (V)	Speed mm/s	Welding pool parameters			
				a (mm)	b (mm)	c_f (mm)	c_r (mm)
Case A	70	9	2	4	3	5	8
Case B	80	9	2	4	3	5	8
Case C	100	9	2	4	3	5	8

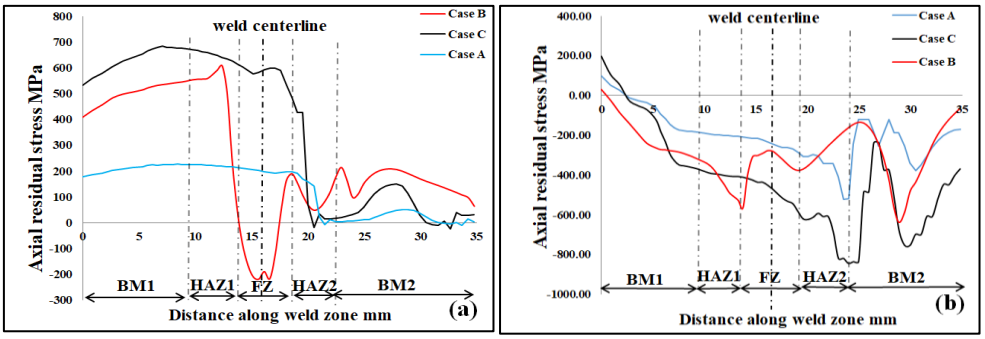

Figure 6. variation of axial residual stress with welding current (a) inner surface (b) Outer surface

6. SUMMARY

From the simulated finite element model, the 2D model was validated using the temperature distribution and hardness test measurement and shows the acceptable agreement. The 2D model for circumferential welding of the pipe is developed and

the residual stresses for outer and inner surfaces are predicted. Axial residual stress changes from tensile to compressive from inner to the outer surface after the welding and the high value found in near and around (HAZ-2) for base metal (P460NH_1). Hoop residual stress changes from tensile to compressive in the outer surface and the high value found in near and around (FZ). The magnitude of residual stress distribution became wider when welding current increases.

REFERENCES

[1] Mobark, H., Lukács, J. (2018). HCF design curves for high strength steel welded joints. *Design of Machines and Structures*, Vol. 8, No. 2, pp. 39–51.

[2] Alhafadhi, Mahmood H., Krallics, György (2019). Numerical simulation prediction and validation two dimensional model weld pipe. *Machines. Technologies. Materials.* Vol. 13, No. 10, pp. 447–450.

[3] Szávai, Sz., Bézi, Z., Rózsahegyi, P. (2016). Material Characterization and Numerical Simulation of a Dissimilar Metal Weld. *Procedia Structural Integrity*, Vol. 2, pp. 1023–1030.

[4] Szávai, Sz., Bézi, Z., Ohms, C. (2016). Numerical simulation of dissimilar metal welding and its verification for determination of residual stresses. *Frattura ed Integrita Strutturale*, Vol. 10, No. 36, pp. 36–45.

[5] Alhafadhi, Mahmood Hasan, Krallics, György (2019). The effect of heat input parameters on residual stress distribution by numerical simulation, iop conference series. Materials Science and Engineering, Vol. 613. No. 1. p. 012035.

[6] Vemanaboina, Harinadh, Akella, Suresh, Buddu, Ramesh Kumar (2014). Welding process simulation model for temperature and residual stress analysis. *Procedia materials science*, Vol. 6, pp. 1539–1546.

[7] Ghosh, P. K., Ghosh, Aritra K. (2004). Control of residual stresses affecting fatigue life of pulsed current gas-metal-arc weld of high-strength aluminum alloy. *Metallurgical and materials transactions*, Vol. 35, No. 8, pp. 2439–2444.

[8] Brickstad, B., Josefson, B. L. (1998). A parametric study of residual stresses in multi-pass butt-welded stainless steel pipes. International journal of pressure vessels and piping, Vol. 75, pp. 11–25.

[9] Deng, Dean, Hidekazu Murakawa, Wei Liang (2008). Numerical and experimental investigations on welding residual stress in multi-pass butt-welded austenitic stainless steel pipe. *Computational Materials Science*, Vol. 42, No. 2, pp. 234–244.

[10] Siddique, M., Abid, M., Junejo, H. F., Mufti, R. A. (2005). 3-D finite element simulation of welding residual stresses in pipe-flange joints: effect of welding parameters. *In materials science forum*, Vol. 490, pp. 79–84.

[11] Goldak, John, Aditya Chakravarti, Bibby, Malcolm (1984). A new finite element model for welding heat sources. *Metallurgical transactions*, Vol. 15, No. 2, pp. 299–305.

Design of Machines and Structures, Vol. 10, No. 1 (2020), pp. 13–19.
Doi: 10.32972/dms.2020.002

THE POSSIBILITIES OF INTELLIGENT MANUFACTURING METHODS

PÉTER FICZERE–NORBERT LÁSZLÓ LUKÁCS

Budapest University of Technology and Economics,
Department of Vehicle Elements and Vehicle-Structure Analysis
1111 Budapest, Stoczek u. 2.
ficzere@kge.bme.hu

Abstract: Additive production technologies made the realization of individually designed, highly complicated geometric structures in practically all fields of industry and human therapy (implantation) possible. In order to minimalize the risk of failure originating from production technology the continuous development of measurements technologies provides the possibility to track the parameters of production and if necessary to ensure their modification. The great number of recorded production data (big data) at the same time can be used in the quality control of the product.

Keywords: *Additive manufacturing, methodology, IoT, i4.0, Remote control for manu-facturers*

1. INTRODUCTION

Nowadays we can hear that we have been living in the fourth industrial revolution. The first industrial revolution was the transition of new manufacturing methods, the transition from hand production to machines, the second was the time of the mass production and the third was time of automation [1]. In case of fourth industrial revolution more technical feature can be highlighted.

Tracking of individual products, monitoring and analysing process of manufacturing conditions and autonomous failure detection can be possible with machine monitoring systems with high quality sensors (for example RFID systems or different measuring systems) and smart industry networks. With assistance of these tools and devices the synergy between smart production lines and information technologies can be put in practice. It means the collection, storing and dispersing of high complexity data which can be set in industrial service by intelligent analysing software. The high volume of data can provide multivarious analysis for different aspects of production [2].

The industrial measuring and data collecting methods have numerous advantages. Places of failures can be predicted and these methods have a significant role in quality assurance (QA). Tracking of products life cycle is a highly recommend task during the production and logistical process. Full transparency in material flow, tracking of production can provide great traceability. With evidence record and store of production data, the identification and certification of individual product can remain

after the delivery. Quality assurance and magisterial tests can be done more economically and quicker [2].

Analysis of data can highly support the sufficient maintenance process and the quick intervention either. The real time online data collection and autonomous failure detection can help the precise manufacturing. For these reasons the amount of waste product can be highly reduced. Continuous data collection can help the verification of certifications.

In the last few years, futurologists and scientist who are involved in the education of design have been studied that which parts of the industry can achieve breakthroughs in the next few years and can affect to everyday life: AI (artificial intelligence), autonomous cars and autonomous manufacturing were predicted as the fifth industrial revolution [3], [4], [5]. Participants of the sixth industrial revolution may can be cyborgs, which means the cooperation of cybernetic and organic beings. In this case we can speak about the hybrids of bits, atoms, gene and nanotechnology.

2. THE POSSIBILITIES OF ADDITIVE MANUFACTURING

Remarkable part of Industry 4.0 is the IoT (Internet of Things) where the equipment is connected in common networks and these instruments can communicate to each other, the big data, where all of data are collected and a more complex analysis is possible with them [6]. Big data can help to time maintenances and some failure can be predicted. The human-machine connection (cobots) come into prominence with the Industry 4.0. Additive manufacturing technologies also must be mentioned, which manufacturing technologies can provide nearly infinite possibilities and produce complex parts in an economical way. [7], [8].

2.1. Additive manufacturing with AI

The newest 3D printers are not bounded to a frame. It means that these machines can change their position, therefore there are no limits with size. These experimental machines can preannounce how will the future look like.

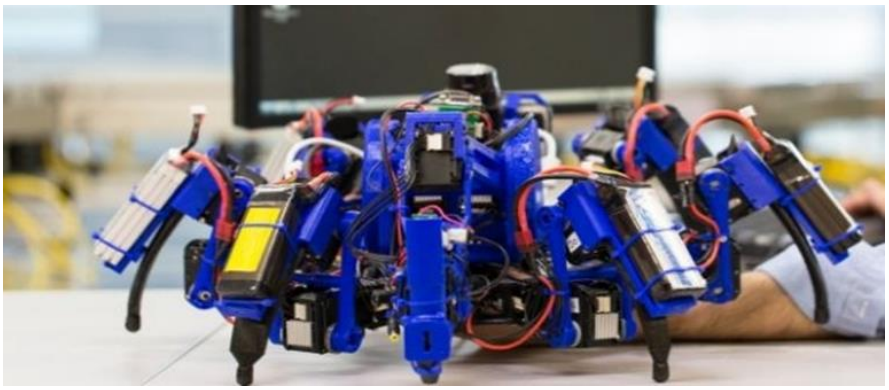

Figure 1. 3D printer spider [9]

In the first picture there is an autonomous 3D printer which operates with the help of artificial intelligence (AI). Every single leg has a 3D printer head and these legs can communicate to each other. These "heads" can solve individual problems and this method is optimised by the communication of them. The sensors in legs can help them to avoid hazards and they also can inform other machines about them. The cooperation of these printers can create functioning products. They can control their own energy consumption and charge themselves if it is needed.

Modern software can optimise the 3D printers and at the same time these systems can pay attention to mechanical properties, accuracy and aesthetics [10]. *Figure 2* shows the influence of adaptive layer height. This function can reduce layer height where it is needed, for example where rounded or complex shaped areas are and allow higher layers for the quicker manufacturing where the resolution is not important.

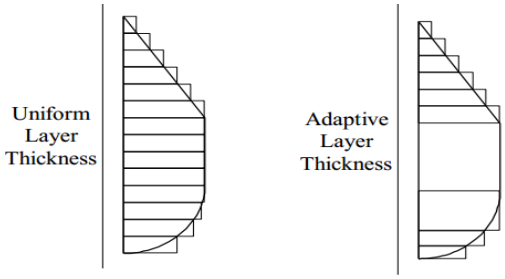

Figure 2. Adaptive layer height [11]

2.2. Diagnostics during the production

As it was mentioned earlier, the certifications during the production are important in quality assurance. For example, EOS can check (metallurgy) and certify every layer during the manufacturing process and therefore these data can be conclusive.

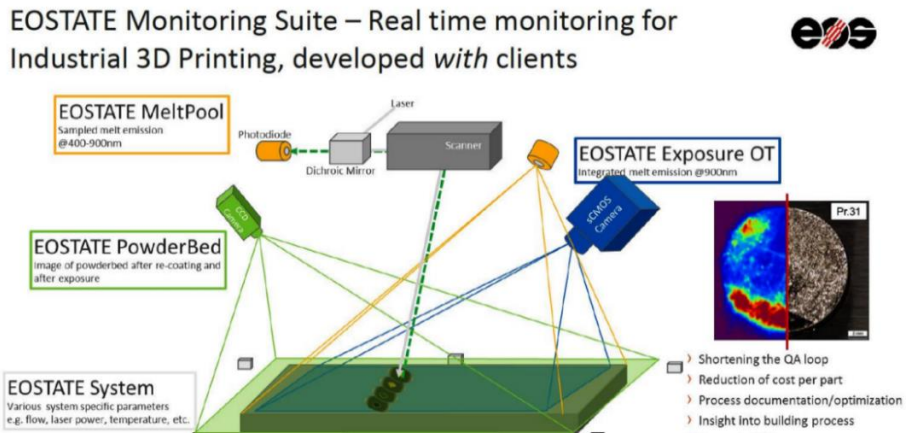

Figure 3. Levels of layer quality control [12]

Nowadays we have the possibility to check and measure the geometrical parameters after every layer, to compare them to the original CAD file. The actual height can also be measured, compared to the actual position, therefore the absolute inaccuracy can be determined and necessary modifications can be executed (i.e.: layer height or temperature can be modified). This possibility can help the intervention and the failures can be prevented automatically. Measuring and intervention methods produce a huge number of data (Big Data) and this is also a part of the Industry 4.0.

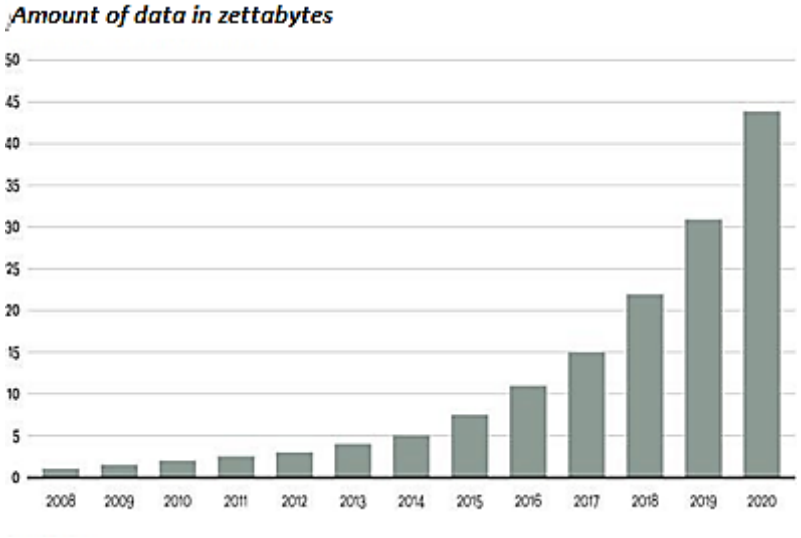

Figure 4. Stored data in each year, in zettabyte [13]

It is also a possibility to measure the amount of material and change it if it is needed. Furthermore, the operator can also choose from the ordered parts depending on the available material and start a print without the risk of material shortage.

2.3. Coordination of machines

Additive manufacturing companies work with more and more 3D printers. In this case it is an enormous challenge to control parallel projects. Nowadays the 3D printers can easily run for 70–80 hours without human intervention, they cannot work independently, without human surveillance. Print endings (if these are not in the working hours) can produce idle time. Remove or of finished products need operators. Complex CAM software can exactly predict the printing time and therefore the projects can be added for proper machines. This assignment can be done online, where the company members can see the status of printers and also can start a new project if the selected machine is available. Furthermore, operators can prevent idle time and provide more profit if the projects will be finished in working hours. In this case, online availability is also useful. This feature is not a privilege of big companies. Some of these systems are available for free for everyone. The actual printing

process can be monitored and possible failures can be detected and solved in real time. This system requires one and more camera and internet (IoT, Internet of Things) what is also a feature of the Industry 4.0. In this case we can intervene during the manufacturing.

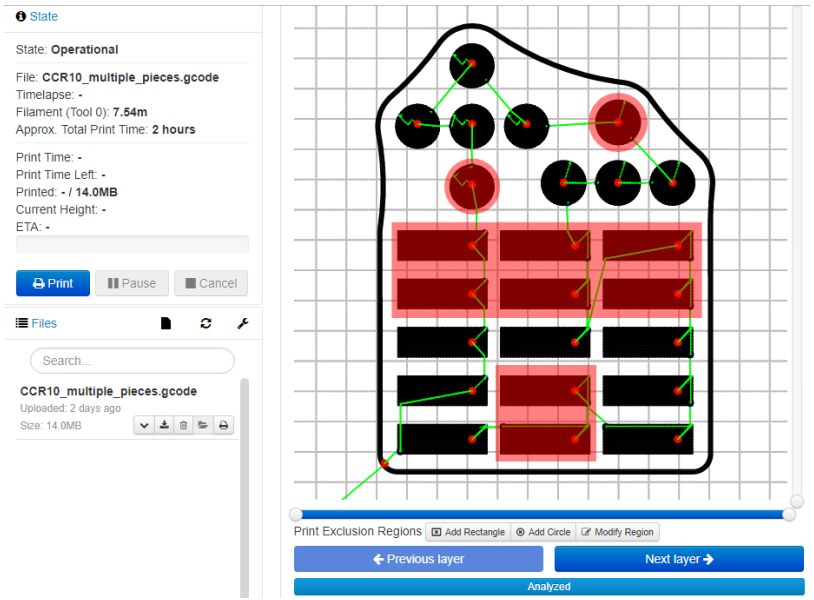

Figure 5. Octoprint [14]

For example, a warped or over crashed part can ruin the whole stack of parts. With the help of this software the failed part (area) can be assigned, then the software can rewrite the g-code and the other parts can be printed uninterruptedly. *Figure 5* shows the software during operation. Assigned areas where the parts will not be printed (red) and parts what will printed normally (black) are noticeable. It can provide less waste, because without this function the complete stack of parts would be spoilage.

3. SUMMARY

Consequently, it is noticeable that just the Industry 4.0 can deal with the more complex demands. For this application the most modern technologies needed. One of these technologies are the additive manufacturing technologies which nowadays more widespread and used are and provide more and more possibilities. Additive manufacturing technologies can utilize the possibilities of Industry 4.0 and production can be more flexible and efficient. These possibilities (IoT, Big Data, etc.) produce more data and these data must be evaluated before storing and using for development.

It is observable that the infrastructure is often available but the human mentality needs recreation. Nowadays the industry needs more flexible thinking for quicker

and economical reactions for challenges of Industry and Economy. It means the use of acquired knowledge is not enough but continuous renewal and development is needed not just for the machine side but for the human side either.

REFERENCES

[1] Ficzere P., Borbás L. (2019). Az ipar 4.0 hatása az egyénre szabható implantáció tervezési folyamatára. *IV. Gépészeti Szakmakultúra Konferencia*, Budapest, Gépipari Tudományos Egyesület, p4, ISBN 978-963-9058-41-5.

[2] http://www.industry4.hu (letöltve 2019. 11. 13.)

[3] Szabó I., Török Á. (2018). Autonóm közforgalmú közösségi közúti gépjárművek társadalmi elfogadtatásának vizsgálata. In: Péter, Tamás (szerk.) *IFFK 2018: XII. Innováció és fenntartható felszíni közlekedés*. Budapest, Magyar Mérnökakadémia (MMA), pp. 333–336, ISBN 978-963-88875-3-5.

[4] Pauer, G., Török, Á. (2019). Static system optimum of linear traffic distribution problem assuming an intelligent and autonomous transportation system. *Periodica Polytechnica Transportation Engineering*, 47 (1), pp. 64–67.

[5] Török, Á., Szalay, Z., Uti, G., Verebélyi, B. (2020). Modelling the effects of certain cyber-attack methods on urban autonomous transport systems, case study of Budapest. *Journal of Ambient Intelligence and Humanized Computing*, 11, pp. 1629–1643, https://doi.org/10.1007/s12652-019-01264-8.

[6] Lekić, M., Rogić, K., Boldizsár, A., Zöldy, M., Török, Á. (2019). Big Data in logistics. *Periodica Polytechnica Transportation Engineeringm*, https://doi.org/10.3311/PPtr.14589.

[7] Ficzere, P., Borbás, L., Török, Á. (2013). Economical investigation of rapid prototyping. *International Journal for Traffic and Transport Engineering*, 3 (3), pp. 344–350, doi: https://doi.org/10.7708/ijtte.2013.3(3).09.

[8] Ficzere P. (2019). Alkatrészek munkatérben történő elhelyezésének a gyártási költségekre gyakorlolt hatása additív gyártástechnológiák esetén. *GÉP*, LXX. évf., 2019/3., pp 26–29.

[9] Livio Dalloro, (head of research group, siemens corporation, corporate technology), Milánó, Italy (2014), https://www.21stcentech.com/spider-robots-bring-portability-autonomy-3d-printing/.

[10] Győri, M., Ficzere, P. (2017). Use of Sections in the Engineering Practice. *Periodica Polytechnica Transportation Engineering*, 45 (1), pp. 21–24, doi: https://doi.org/10.3311/PPtr.9144.

[11] Broek, Johan J., Horváth, Imre, de Smit, Bram, Lennings, Alex F., Vergeest, Joris S.M. (1998). *A Survey of the State of Art in Thick Layered Manufacturing*

of Large Objects and the Presentation of a Newly Developed System. University of Texas at Austin.

[12] Falk Gy. (2019). Az asztali és az ipari fémnyomtatás közötti különbségek. Előadás. *Ipar Napjai – Mach-Tech*, Budapest, 2019. május 16.

[13] What is Hadoop? https://www.sas.com/en_us/insights/big-data/hadoop.html (letöltve: 2019. 12. 17.).

[14] https://plugins.octoprint.org/plugins/excluderegion (letöltve: 2020. 02. 15.).

Design of Machines and Structures, Vol. 10, No. 1 (2020), pp. 20–27.
Doi: 10.32972/dms.2020.003

CONTROL OF A CABLE ROBOT ON PSOC CYPRESS PLATFORM

PÁLMA KAPITÁNY[1]–JÓZSEF LÉNÁRT[2]*

[1] Robert Bosch Department of Mechatronics,
Faculty of Mechanical Engineering and Informatics
University of Miskolc, Egyetemváros, H-3515 Miskolc, Hungary,
e-mail: kapitanypalma@gmail.com
[2] Robert Bosch Department of Mechatronics,
Faculty of Mechanical Engineering and Informatics
University of Miskolc, Egyetemváros , H-3515 Miskolc, Hungary,
e-mail: lenart.jozsef@uni-miskolc.hu

Abstract: This paper deals with the control of a cable model robot. The continuous motion of the end effector is provided by velocity control of four DC motors. In each uniform time step the rotational speed of the motors are predicted based on the assumption of constant path velocity of the end effector in order to move it to prescribed position. In the next time step the rotational speed of the motors are calculated from the difference between the actual position and the target one. This way the discrepancy between the actual position and the prescribed one is corrected step-by-step. The control algorithm is implemented on Cypress Semiconductor CY8CKIT PSoC 5LP microcontroller.

Keywords: *Cable robot, Velocity control of DC motors, Microcontroller, Inverse kinematics*

1. INTRODUCTION

Cable robots are frequently used e.g. to move cameras in sport halls and stadiums and for logistics in high stores [1]. Big working space and fast positioning are the advantages of cable robots. There are two main groups of cable robots planar ([5], [6]), and spatial ones ([7], [8]).

The most important purpose of the plane movers is the precise positioning, it is utilized in cable drawing machines, in industrial applications they carry out logistical tasks, or external cleaning of office buildings. 3D cable robots are capable of not only positioning, but can also control the orientation of the end-effector being moved. Robots are popular in the airplane industry, because they can follow complicated spatial shape when welding wing elements, similarly to painting.

Nowadays it is also used for nonindustrial purposes, e.g., flight simulation, theatrical performances, solar panel assembly, and health rehabilitation exercises, etc. [1].

* Corresponding Author

In a previous article [2], the authors of this paper published a test bench that approximated a curve path by a polygon. Four DC motors were controlled with one master and four slave microcontrollers. The motion of the end-effector was non-continuous, because the master waited for the slaves to finish their tasks in each increment, i.e., to perform the motion along one polygon side.

This robot has been upgraded, with the complete replacement of the control unit by a single Cypress Semiconductor CY8CKIT PSoC 5LP microcontroller. As a result of the current research it has a continuous speed control. It is checking the predicted progress at each time step. When the length of the cables are lagging behind the calculated values the speed of the motors are increased, and vice versa.

The organization of this paper is as follows. In Section 2, the inverse kinematics of the robot is discussed. In Section 3, the control of the four motors are described. Finally, summary is given in Section 4.

2. INVERSE KINEMATICS

Figure 1 shows the picture of a planar cable robot. The end effector is suspended by four cables, which are winded on winches. The winches are driven by four DC motors identified by letters *a, b, c, d*. The displacement increment of the end effector is sketched in *Figure 2*. The end-effector of cable robot denoted by blue disc is moved in plane xy.

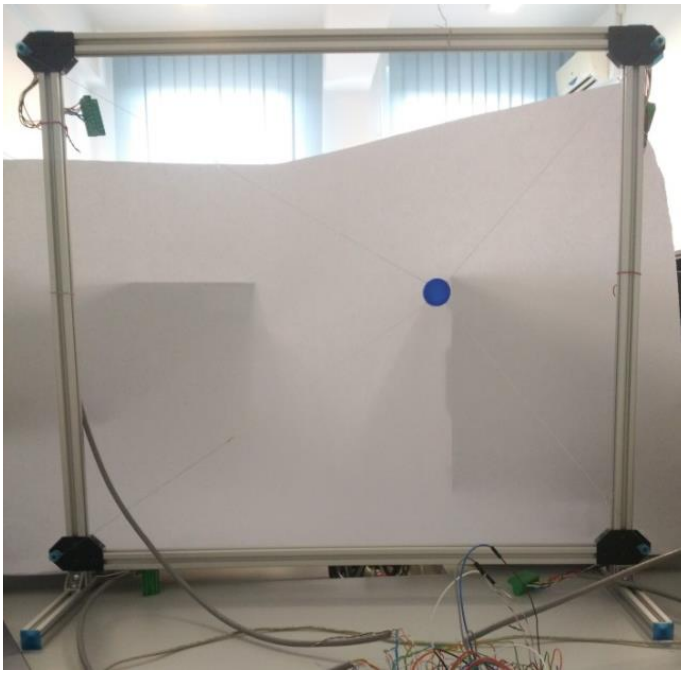

Figure 1. Planar cable robot

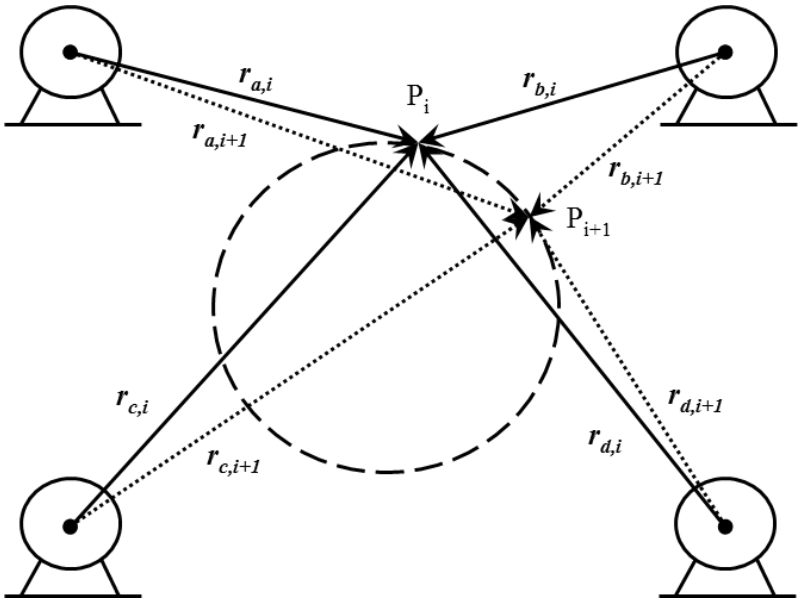

Figure 2. Displacement increment

The task of the inverse kinematics is to determine the four cable lengths for any position of the end-effector. To perform a prescribed path of the end-effector starting from a null point the length of suspending cables can be prescribed by functions. The control is not continuous, but it is performed step by step with sampling time Δt. The changes in lengths of the cables during a time step are determined by measured signals of the motor encoders.

Figure 2 shows a circular path of the end-effector. The control of the motion is based on a frequently repeated predictor algorithm, which recalculates the prediction from the instantaneous position.

The points of the planned circular path are determined by the following equation:

$$x[i] = x_k + r_k \cdot \cos\left(\frac{i \cdot 2\pi}{n_o}\right), \tag{1}$$

$$y[i] = y_k + r_k \cdot \sin\left(\frac{i \cdot 2\pi}{n_o}\right), \tag{2}$$

where r_k x_k and y_k are respectively the radius, the horizontal and vertical coordinates of the center of the circle, $x[i]$ and $y[i]$ are the horizontal and vertical coordinates of a point i of the circle path, n_o is the number of the sides of the polygon approximating the circle.

For the control the end points i and i + 1 coordinates of the polygon are required to determine the target cable length for the corresponding motor:

$$r_{a,i} = K \cdot \sqrt{x[i]^2 + y[i]^2}, \tag{3}$$

$$r_{b,i} = K \cdot \sqrt{(x[i] - h)^2 + y[i]^2}, \tag{4}$$

$$r_{c,i} = K \cdot \sqrt{x[i]^2 + (y[i] + v)^2}, \tag{5}$$

$$r_{d,i} = K \cdot \sqrt{(x[i] - h)^2 + (y[i] + v)^2}, \tag{6}$$

$$r_{a,i+1} = K \cdot \sqrt{x[i+1]^2 + y[i+1]^2}, \tag{7}$$

$$r_{b,i+1} = K \cdot \sqrt{(x[i+1] - h)^2 + y[i+1]^2}, \tag{8}$$

$$r_{c,i+1} = K \cdot \sqrt{x[i+1]^2 + (y[i+1] + v)^2}, \tag{9}$$

$$r_{d,i+1} = K \cdot \sqrt{(x[i+1] - h)^2 + (y[i+1] + v)^2} \tag{10}$$

where for the point *i*: $r_{a,i} - r_{d,i}$ are the cable lengths measured from motors *a – d*, *h* is the width and *v* is the height of the working space, *K* is a constant depending on the gear ratio, encoder signals per revolution and reel radius. For point *i + 1* the corresponding variables are denoted in similar way.

The predicted signal frequencies of the encoders for motor *a-d* are calculated as:

$$f_a = \frac{r_{a,i} - r_{a,i+1}}{\Delta t} \tag{11}$$

$$f_b = \frac{r_{b,i} - r_{b,i+1}}{\Delta t} \tag{12}$$

$$f_c = \frac{r_{c,i} - r_{c,i+1}}{\Delta t} \tag{13}$$

$$f_d = \frac{r_{d,i} - r_{d,i+1}}{\Delta t} \tag{14}$$

where Δt is the sampling time, which is set by the user.

PWM values of the motors *a–d* are determined by $f_a - f_d$ using linear interpolation based on measurements. It is noted that a DC motor requires a minimal voltage to start and the relation between the rotational speed and voltage is not perfectly linear.

Figure 3 demonstrates the strategy of the repeated prediction method, where dashed line denotes the ideal cable length curve as a function of time. Dot-dash lines represent the predicted change of the cable length while thin solid lines give the performed length of the cable, which is a string polygon.

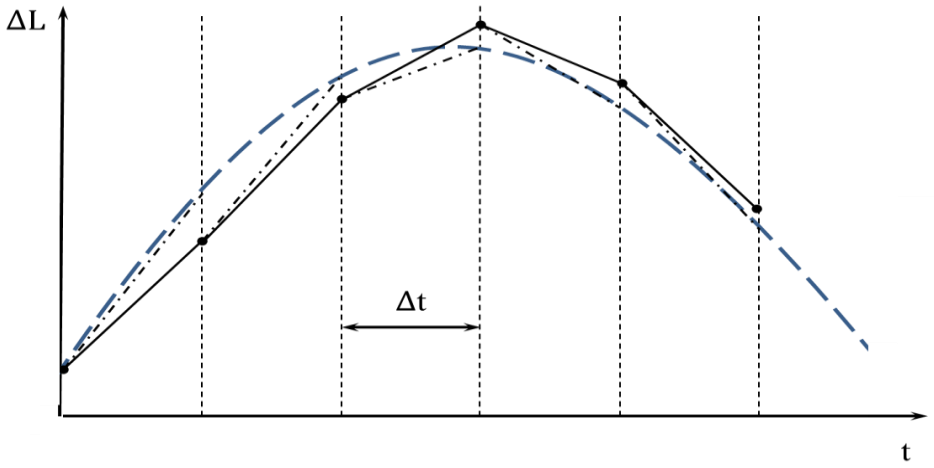

Figure 3. Strategy of the repeated prediction method

3. CONTROL AND PROGRAMMING ON PSOC

The Cypress Semiconductor CY8CKIT PSoC 5LP microcontroller was chosen for the development of the proposed control system because it can process four PWM blocks, four Quadrature Decoders, a Timer and four Control Registers at the same time. Further advantage is that each of the inputs and outputs can be arbitrarily set to digital or analog, the number of all pins is 46. The program and logic design are written in a PSoC Creator 4.2 designer program, which has a user friendly interface.

Velocities of the motors are set through H-Bridges via PWM values. The direction of rotation is controlled by two digital outputs through H-Bridges. Position of the end-effector can define with encoder signals, which are two digital inputs for the Quadrature Decoder function block for each motor. The microcontroller, PWM blocks and Quadrature Decoders work with 24 MHz, 125 kHz and 12 MHz, respectively. Interrupt output signal of the timer is set to 0.3 second as a result of optimization. This time step is short enough to achieve a high accuracy and it provides a smooth motion. The UART and LED help to check the process. *Figure 4* shows the structure of control system in PSoC Creator 4.2.

Interrupt signal of the timer makes a step by step velocity correction based on the actual position. *Figure 5* presents the program process with respect the priority. The definitions, path approximation, PWM values calculation and start of function block are called in the main program. When the timer counter is full it sends an interrupt signal, which starts the interrupt program part. In this program part the controller recalculates the velocity values based on actual position and refresh the PWM outputs. Then the pointer is jumping to the next command of the main program to continue it. Hardware of the control system is shown in *Figure 6*.

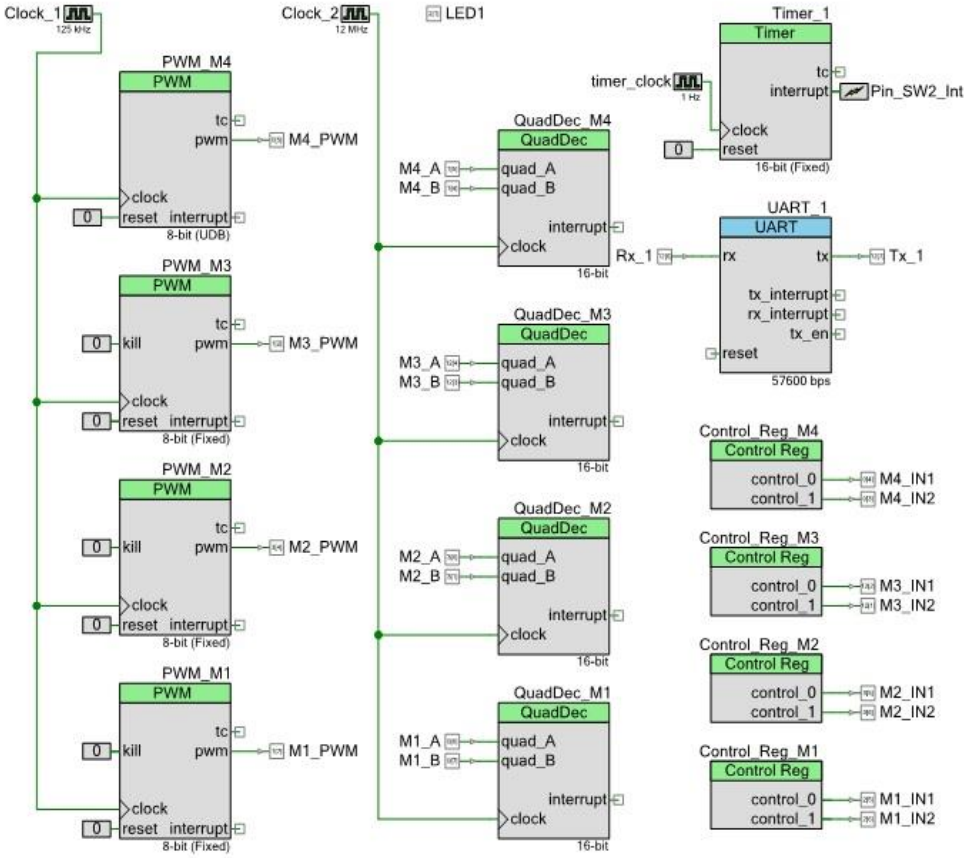

Figure 4. Structure of control system in PSoC Creator 4.2

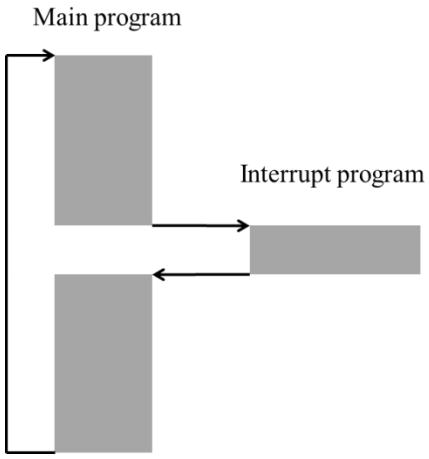

Figure 5. Interrupt handling structure

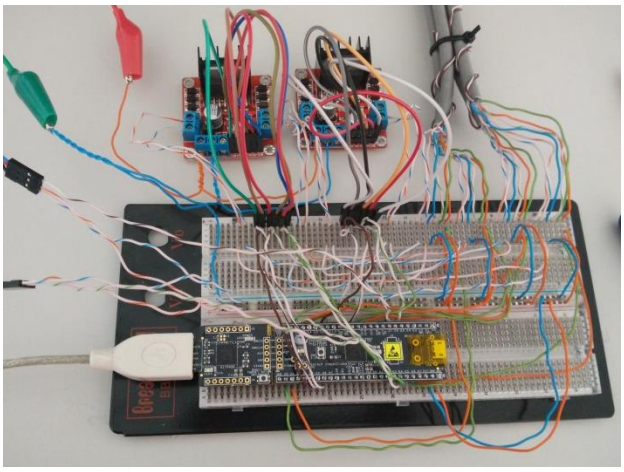

Figure 6. Hardware of the control system on breadboard

4. SUMMARY

This paper dealt with a 2D cable robot. The end-effector driven by four DC motors, which are controlled by a single PSoC Cypress microcontroller. The path of the end-effector is prescribed by a string polygon of uniform sections. The goal is to move the end-effector along sections of the polygon step-by-step. The strategy of the control based on the difference between the actual position and the prescribed polygon position. The program computes the increments in the cable lengths, which determine the PWM values for corresponding motors. This method provides a smooth, continuous motion of the end-effector.

ACKNOWLEDGEMENTS

The described article was carried out as part of the EFOP-3.6.1-16-2016-00011 *Younger and Renewing University – Innovative Knowledge City – institutional development of the University of Miskolc aiming at intelligent specialisation* project implemented in the framework of the Szechenyi 2020 program. The realization of this project is supported by the European Union, co-financed by the European Social Fund.

REFERENCES

[1] Bruckmann, T., Lalo, W., Sturm, C. (2013). Application examples of wire robots. *Multibody System Dynamics, Robotics and Control, Workshop on Multibody System Dynamics, Robotics and Control*, Linz, 26–27 September 2011, Gattringer, Hubert, Gerstmayr, Johannes, pp. 291–310.

[2] Kapitány, P., Lénárt, J. (2019). Kinematics and control of a planar cable robot. *International Journal of Engineering and Management Sciences (IJEMS)*, Vol. 4, No. 1, pp. 88–95.

[3] Bruckmann, T., Pott, A., Franitza, D., Hiller, M. (2006). A Modular Controller for Redundantly Actuated Tendon-Based Stewart Platforms. *The first European Conference on Mechanism Science*, Obergurgl, Austria, 21–26 February 2006.

[4] Jadhao, K. S., Lambert, P., Bruckmann, T., Herder, J. L. (2018). Design and Analysis of a Novel Cable-Driven Haptic Master Device for Planar Grasping. In: Gosselin, C., Cardou, P., Bruckmann, T., Pott, A. *Cable-Driven Parallel Robots. Mechanisms and Machine Science*. Vol. 5, Cham, Switzerland.

[5] Xue Jun Jin, Dae Ik Jun, Pott, A., Sukho Park, Jong-Oh Park, Seong Young Ko (2013). Four-cable-driven parallel robot. *13th International Conference on Control, Automation and Systems*, Kimdaejung Convention Center, Gwangju, Korea.

[6] Gosselin, C., Ren, P.,Foucault, Simon (2012). Dynamic Trajectory Planning of a Two-DOF Cable-Suspended Parallel Robot. *Proceedings – IEEE International Conference on Robotics and Automation*, pp. 1476–1481, 10.1109/ICRA.2012.6224683.

[7] Gosselin, C., Foucault, S. (2015). Experimental Determination of the Accuracy of a Three-Dof Cable-Suspended Parallel Robot Performing Dynamic Trajectories. *Mechanisms and Machine Science*, 32, pp. 101–112, 10.1007/978-3-319-09489-2_8.

[8] Lau, D., Hawke, T., Kempton, L., Oetomo, D., Halgamuge, S. (2010). Design and Analysis of 4-DOF Cable-Driven Parallel Mechanism. *Proceedings of the 2010 Australasian Conference on Robotics and Automation*.

Design of Machines and Structures, Vol. 10, No. 1 (2020), pp. 28–38.
Doi: 10.32972/dms.2020.004

MISMATCH EFFECT ON FATIGUE CRACK PROPAGATION LIMIT CURVES OF GMAW JOINTS MADE OF S960QL AND S960TM TYPE BASE MATERIALS

HAIDAR MOBARK[1]–JÁNOS LUKÁCS[2]

Institute of Materials Science and Technology,
Faculty of Mechanical Engineering and Informatics, University of Miskolc [1, 2]
H-3515, Miskolc-Egyetemváros
mobark.mechanical@gmail.com[1], janos.lukacs@uni-miskolc.hu[2]

Abstract: Welded structures cannot be produced without imperfections, cracks or crack like defects. Among the structural steels, 960 MPa strength category represents a reliable application possibility. Consumables are also available, but the behaviour of mismatch types under cyclic loading condition is not yet clear. In order to know the fatigue crack propagation resistance of 960 MPa strength category steels and their gas metal arc welded joints fatigue crack growth tests were performed. The tests results were analysed and fatigue crack propagation limit curves were determined.

Keywords: *high strength steel, gas metal arc welding, mismatch, fatigue crack growth, limit curve*

1. INTRODUCTION

The term fatigue was mentioned for the first time by Braithwaite (1854); he described many service fatigue failures. In 1870 Wöhler presented his law (Wöhler law), based on investigations of railway axles. He composed as follows: *"Material can be induced to fail by many repetitions of stresses, all of which are lower than the static strength. The stress amplitudes are decisive for the destruction of the cohesion of the material. The maximum stress is of influence only in so far as the higher it is, the lower are the stress amplitudes which lead to failure"*. Wöhler's successor presented the S-N curve (1936), it is called Wöhler curve, and Basquin represented the finite life region of the curve and described it by a simple formula (σ = stress, N = number of cycles, a, b = material parameters):

$$\sigma = aN^b. \tag{1}$$

Afterwards Bauschinger mentioned for fatigue by his sentence *"the change of the elastic limit by often repeated stress cycles"*. The first experiments to improve the fatigue strength of components were carried out in the U.K. during the First World War [1].

From 1960 onwards the number of fatigue experts increased still further. This must also be attributed to the rapid development of fracture mechanics, i.e. of fatigue-crack propagation. Paris established that fatigue crack propagation could be described by the following equation (da/dN = fatigue crack growth, ΔK = stress intensity factor range, C, n = material constants) [2, 3]:

$$\frac{da}{dN} = C\Delta K^n, \tag{2}$$

which equation soon set out on a veritable triumphant advance around the world [1]. The complex process of crack propagation is undoubtedly described much too simply by this equation; this fact however did not prevent its – either undiscriminating or adding further characteristics – use all over the world to this very day.

The most commonly used structural material for the construction of engineering structures is steel, and the most widely used joining technology is welding. Nowadays, steel providers create a modern version of a high-strength base materials and filler metals with yield strength start from 690 MPa and up. However, high strength lightweight structures with low cost of steel weldments lead to apply in many manufacturing aspects (e.g. mobile cranes, hydropower plants, offshores, trucks, earth-moving machines, and drums), because of an extensive reduction in weight [4].

As in *Figure 1* (a) [5] can be seen, the interaction of load, material, and design represents reliability of welded components. A superposition of local and global welding stresses may lead to high residual stress levels which are able to reduce the components safety *[*see *Figure 1 (b)]* [6].

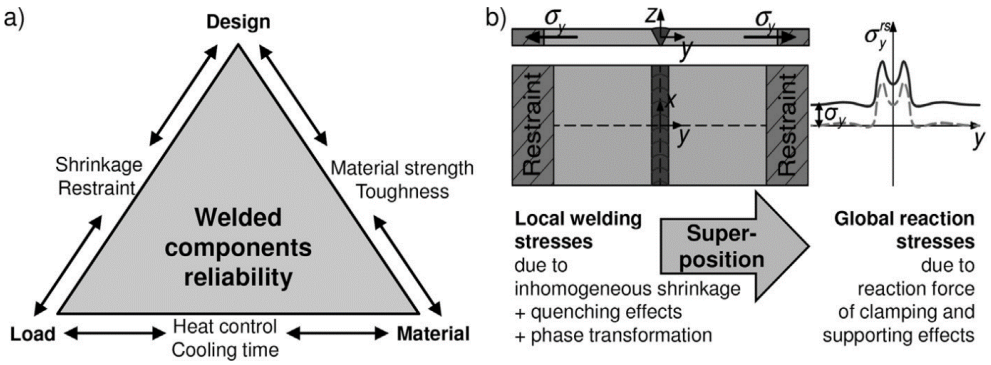

Figure 1. Interaction of design, material and load (a) during component production and service [5]*; welding stresses as a result of local and global restraint (b)* [6]

Welded joints are very sensitive parts of structures, because the welded regions are in complex metallurgical and stress conditions. Before the Second World War, the

design of all engineering structures was based on yield/tensile strength and ductility. Mild steel was used as the structural material and the minimum yield strength of the weld metal was found to be around 340 MPa. The yield strength to tensile strength ratio of the weld metals that were used for welding the mild steel in early designs was very high and the designers did not pay much attention to the yield strength of the weld metals. It has been reported that the maximum yield strength of the filler metal that has been used for joining the mild steel plates was about 59% higher than the base material [7].

High strength structural steels (HSSS) with yield strengths from 690 MPa upwards are applied in growing amount in industrial applications. Specific design solutions and economic aspects of modern steel constructions lead to an increasing trend in light-weight design. Steel producers currently provide a diversified spectrum of high-strength base materials and filler metals. Thus an extensive reduction in weight and production costs can be achieved with increasing material strength [4]. During the welding process the joining parts are affected by heat and force, which cause inhomogeneous microstructure and mechanical properties, and furthermore stress concentrator places can form. Both the inhomogeneity of the welded joints and the weld defects play important role in case of cyclic loading conditions. High cycle fatigue (HCF) and fatigue crack growth (FCG) phenomena are a very common problem in welded structures; however, there are a limited knowledge about the fatigue behaviour of HSSS base materials and welded joints up to now. In accordance with the welding challenges nowadays, the mismatch effect should be examined too [8, 9].

The research work is a significant continuation of previous researches, builds upon their experience [9] and uses their measurement results [10, 11]. Hereupon the aims of this paper are as follows:

- characterisation the FCG resistance of different high strength steels in 960 MPa strength category and their gas metal arc welded (GMAW) joints;
- investigation of the mismatch effect and the heat input on the FCG behaviour of the GMAW joints;
- determination of FCG limit curves for the investigated steels and their GMAW joints, based on the simple crack growth relationship [12].

2. MATERIALS, WELDING AND TESTING CIRCUMSTANCES

The chemical composition and the basic mechanical properties of the investigated base materials (BM) and filler metals (FM) are summarized in *Tables 1–2*, respectively. (The used abbreviations are as follows: Weldox 960E = W9E, Alform 960M = A9M, Union X90 = U90, Union X96 = U96, WJ = welded joint, W9E-BM = base material was tested, W9E-WJ = welded joint made out of this base material was tested.)

Table 1
The chemical composition of the investigated base materials and filler metals (weight%)

ID	C	Si	Mn	P	S	Cr	Ni	Mo
W9E-BM	0.16	0.22	1.24	0.009	0.001	0.19	0.05	0.581
W9E-WJ	0.16	0.23	1.25	0.008	0.001	0.20	0.04	0.605
A9M	0.084	0.329	1.65	0.011	0.0005	0.61	0.026	0.29
U90	0.1	0.8	1.8	N/A	N/A	0.35	2.3	0.6
U96	0.1	0.81	1.94	0.015	0.011	0.52	2.28	0.53
ID	**V**	**Ti**	**Cu**	**Al**	**Nb**	**B**	**N**	**Zr**
W9E-BM	0.041	0.004	0.01	0.056	0.016	0.001	0.003	N/A
W9E-WJ	0.04	0.004	0.01	0.06	0.016	0.001	0.003	N/A
A9M	0.078	0.014	0.016	0.038	0.035	0.0015	0.006	N/A
U90	N/A	N/A	N/A	N/A	N/A	N/A	N/A	N/A
U96	< 0.01	0.06	0.06	< 0.01	N/A	N/A	N/A	< 0.01

Table 2
The mechanical properties of the investigated base materials and filler metals

ID	s / d mm	$R_{p0.2}$ MPa	R_m MPa	A %	CVN impact energy J
W9E-BM	15	1007	1045	16.0	−40 °C: 141
W9E-WJ	20	1007	1053	16.0	−40 °C: 105
A9M	15	1051	1058	16.9	−40 °C: 40
U90	1.2	≥890	≥950	≥15.0	−60 °C: ≥47; 20 °C: ≥90
U96	1.2	≥930	≥980	≥14.0	−50 °C: ≥47; 20 °C: ≥80

GMAW process was applied, matching (M) and undermatching (UM) mismatch conditions were selected for the studying of BM and FM pairing, as follows: W9E-U96 = M, A9M-U90 = UM and A9M-U96 = M. Medium heat input (m) was used during the welding, except for A9M-U90 = UM, where high heat input (h) was applied, too. The welding equipment was a DAIHEN VARSTROJ WELBEE P500L power source. The dimensions of the welded plates were 300 mm × 125 mm. For the equal stress distribution double V-grooved welding joints were used, with 80° groove angle, 2 mm root opening, and 1 mm land thickness. During the welding, the test pieces were rotated after each layer. Based on the industrial practice, solid wires and 18% CO_2 + 82% Ar gas mixture (M21) were applied in all cases. The root layers (2 layers for both thicknesses) were made by a qualified welder; while the other

layers (6 layers for 15 mm and 10 layers for 20 mm thicknesses) were made by automated welding car. The welding parameters (preheating and interpass temperatures (T_{pre} and T_{ip}), current (I), voltage (U), welding speed (v_w), linear energy E_v), cooling time ($t_{8.5/5}$)) were selected based on both theoretical considerations and real industrial applications, and were summarized in *Table 3*. (The used abbreviations are as follows: root = r, filler = f).

Table 3

The applied welding parameters during our investigations

ID	Layer	T_{pre},T_{ip} °C	I A	U V	v_w cm/min	E_v J/mm	$t_{8.5/5}$ s
W9E/m	1 r	200	96	17.3	11	727	6.7
	2 r	180	194	22.0	27	764	6.5
	3–12 f	150	298–308	29.0–31.0	45	940–1000	7–8
A9M/m	1–2 r	70	135–150	20.0–20.7	20	675–740	4.9–6.3
	3–8 f	180	290–295	27.5–29.0	40	900–1020	7.5–9.0
A9M/h	1–2 r	70	135–145	17.5–18.0	20	565–630	4.0–9.6
	3–8 f	300	270–300	27.5–29.0	40	890–1050	14.5–18.0

The FCG tests were executed on three-point bending (TPB) specimens, nominal W values were 13 / 18 mm and 26 / 28 mm for both base materials and welded joints. The position of the notches in the base materials correlated with the rolling direction (indicated: T-L, L-T, T-S, and L-S), and in the welded joints with the 21 and 23 joint directions (indicated: 21 W and 23 W). The notch locations, the notch distances from the centreline of the welded joints, were different; therefore, the positions of the notches and the crack paths represent the most important and the most typical crack directions in a real welded joint (statistical approach). Post-weld heat treating was not applied after welding on GMAW joints (investigations in as-welded condition). The FCG examinations were performed with tensile stress, R = 0.1 stress ratio, sinusoidal loading wave form, at room temperature, and on laboratory air, using MTS type electrohydraulic testing equipment. The loading frequency was different, it was f = 20 Hz at the two-thirds of crack growth, and it was f = 5 Hz at the last third. The propagating crack was registered with optical method, using video camera and hundredfold magnification (N = 100x).

3. RESULTS

Vickers hardness (HV10) and hardness distributions were measured on both joint directions; the structure of the welded joints can be seen in *Figure 2*, and *Figure 3* shows the hardness distributions in case of A9M-U90, which clearly demonstrates the influence of the undermatched filler metal.

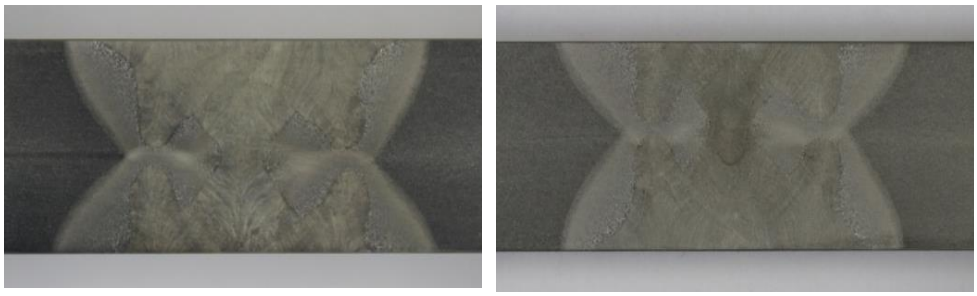

Figure 2. T-L/21W and T-S/23W specimens for hardness tests in case of A9M-U90

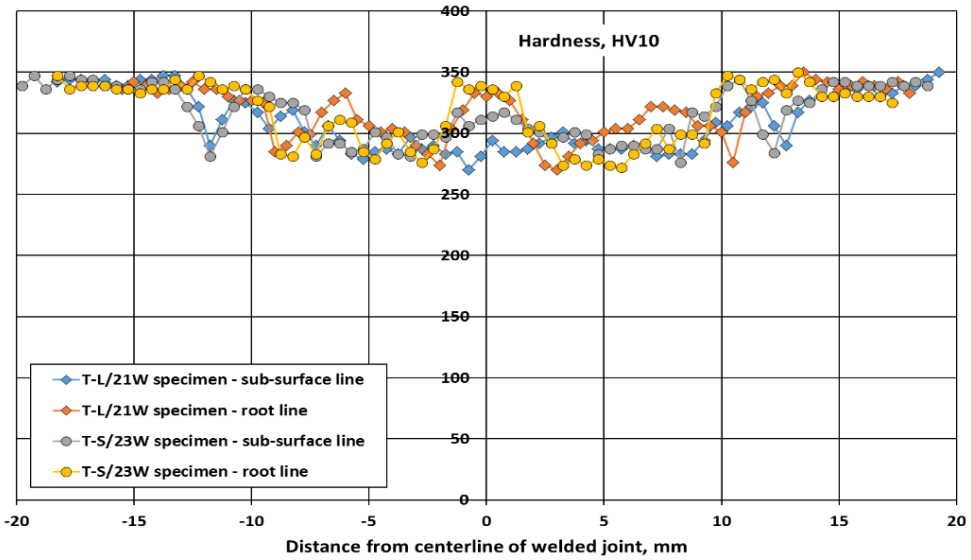

Figure 3. Hardness distributions in case of A9M-U90

The crack length vs. number of cycles curves (a-N) for A9M-U90 pairing (under-matching case) and high heat input (h) can be seen in *Figure 4* (T-L/21W orientation) and *Figure 5* (T-S/23W orientation).

Secant method [13] was used to evaluate the fatigue crack growth data. *Figure 6* introduces the calculated fatigue crack growth rate vs. stress intensity factor range values, in both orientations. The constants (C and n) of the Paris *equation (2)* were calculated using the least squares regression method and the fatigue fracture toughness (ΔK_{fc}) values were determined using the crack length on the crack front measured by stereo microscope. The data not belonging to stage II of the kinetic diagram of fatigue crack propagation have been eliminated during the least square regression analysis, for each specimen, systematically. The calculated values and the correlation coefficients were summarized in *Table 4*.

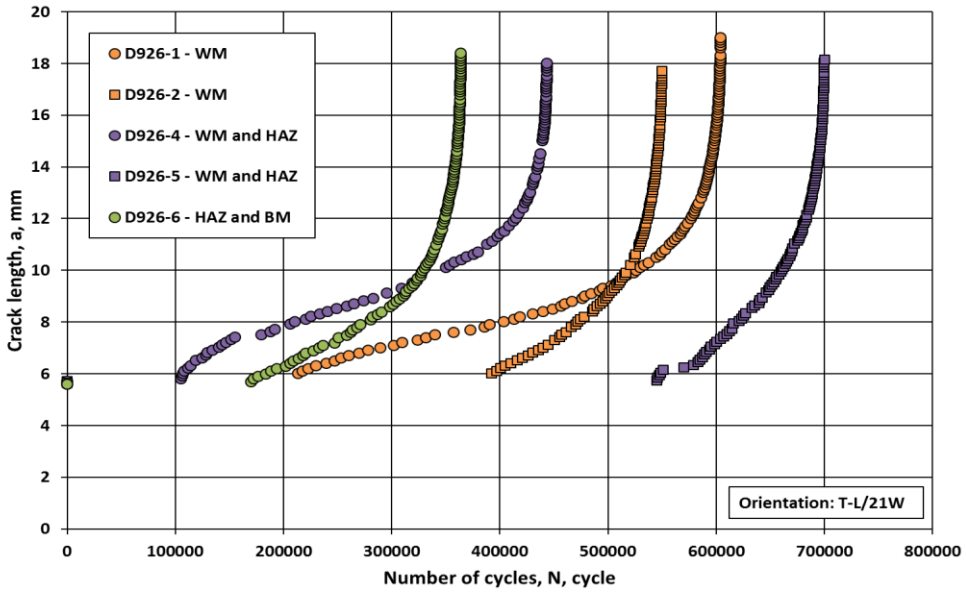

Figure 4. Crack length vs. number of cycles curves for A9M-U90 pairing in T-L/21W orientation

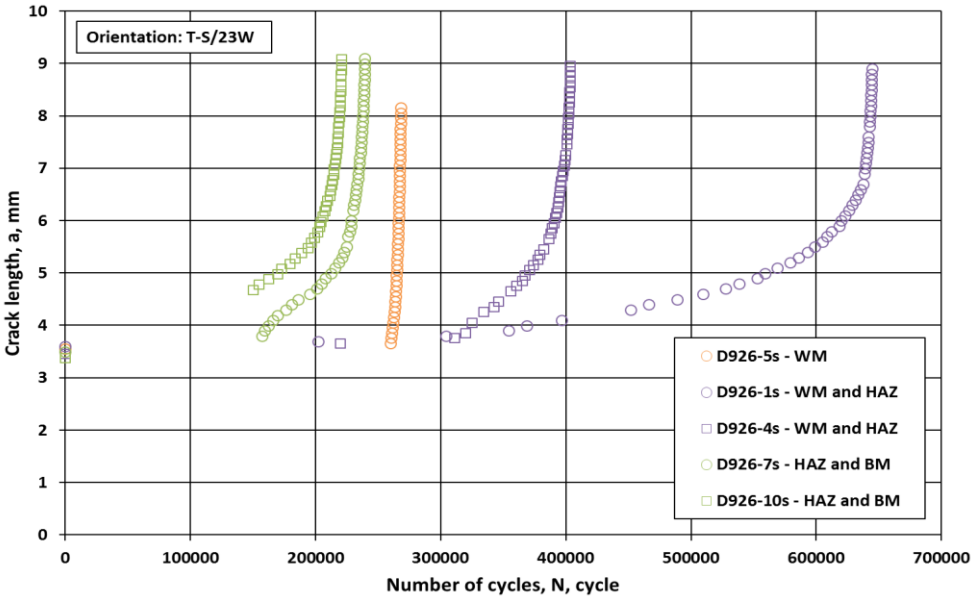

Figure 5. Crack length vs. number of cycles curves for A9M-U90 pairing in T-S/23W orientation

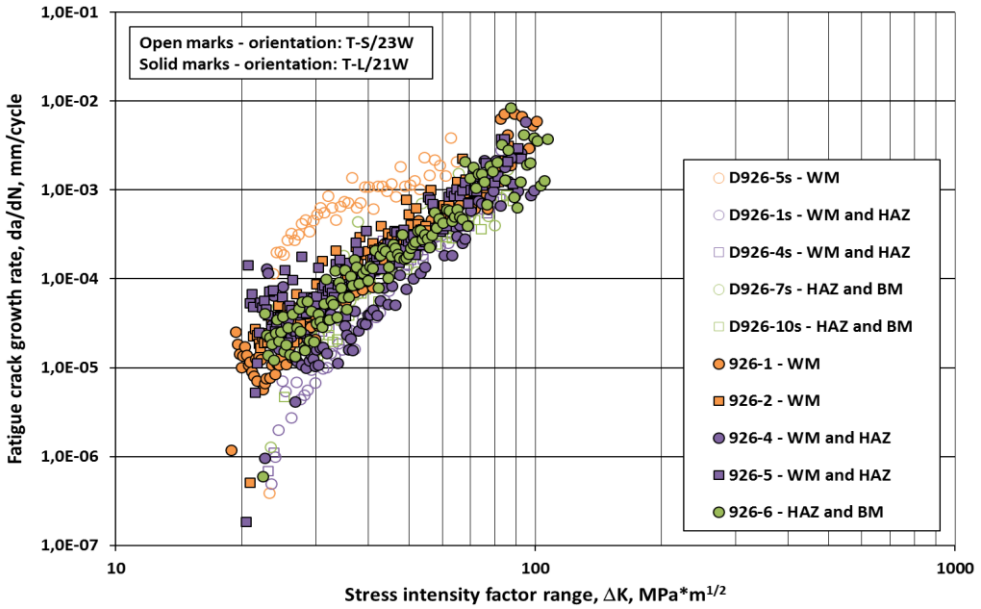

Figure 6. Kinetic diagrams of fatigue crack propagation for A9M-U90 pairing in both investigated orientations

Table 4

The two constants of the Paris equation and the fatigue fracture toughness values for each specimen in case of A9M-U90 pairing

Specimen ID	Crack path	n	C	Correlation coefficient	ΔK_{fc}
		mm/cycle, MPam$^{1/2}$		–	MPam$^{1/2}$
Specimen location: T-S/23W					
D926-5s	WM	2.108	3.605E-07	0.9134	66.9
D926-1s	WM and HAZ	5.122	2.450E-13	0.9768	86.2
D926-4s	WM and HAZ	3.282	4.885E-10	0.9549	88.5
D926-7s	HAZ and BM	3.298	5.483E-10	0.9202	92.5
D926-10s	HAZ and BM	3.982	2.709E-11	0.9642	91.9
Specimen location: T-L/21W					
D926-1	WM	3.855	6.831E-11	0.9795	103.1
D926-2	WM	3.362	6.727E-10	0.9727	87.8
D926-4	WM and HAZ	4.499	2.739E-12	0.9674	101.3
D926-5	WM and HAZ	3.024	2.372E-09	0.9446	94.4
D926-6	HAZ and BM	3.588	2.031E-10	0.9636	109.2

Based on the experimental data and results, fatigue crack propagation limit curves were determined using a previously developed six steps method [14]. *Table 5* summarizes the parameters of the determined fatigue crack propagation limit curves and *Figure 7* demonstrates the curves for all cases.

Table 5
Characteristics of the determined fatigue crack propagation limit curves

ID	Orientation	n	C	ΔK_{fc}	Source
		mm/cycle, $MPa^{1/2}$		$MPa^{1/2}$	
W9E-BM	T-S, L-S, T-L	1.80	3.50E-07	94	[11]
W9E-U96/m	T-L/21W, T-S/23W	2.75	1.03E-08	93	[11]
A9M-BM	T-L, L-T	1.82	4.63E-07	116	[10]
	T-S	1.75	6.41E-07	87	[10]
A9M-U90/m	T-L/21W	2.40	3.10E-08	115	[10]
	T-S/23W	2.15	9.93E-08	67	[10]
A9M-U90/h	T-L/21W, T-S/23W	2.65	1.65E-08	81	this study
A9M-U96/m	T-L/21W	1.90	3.19E-07	114	[10]
	T-S/23W	2.75	6.06E-09	82	[10]

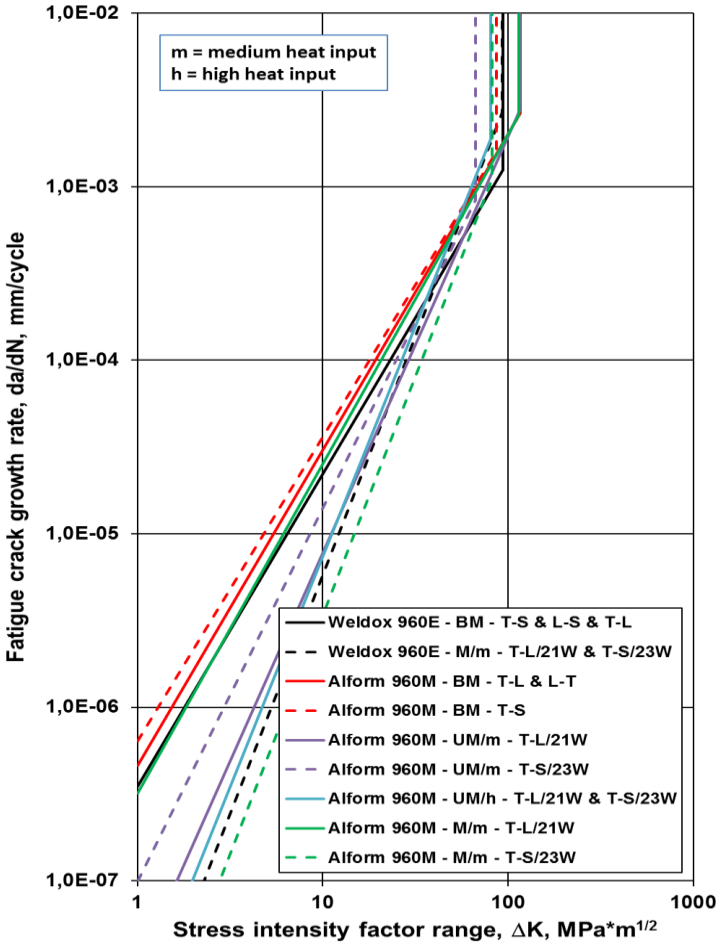

Figure 7. Determined fatigue crack propagation limit curves for 960 MPa strength category steels and their welded joint

4. Summary and conclusions

Based on our investigations, the calculated and analysed testing results, and the accomplished comparisons, the following conclusions can be drawn.

The results of the achieved fatigue crack growth investigations justified the necessity of statistical approaches, especially referring to the directions of the base materials and the welded joints, and the determination of the number of the tested specimens.

The applied gas metal arc welding process and the used technological parameters are suitable for production welded joints with appropriate quality, where the appropriate quality contains the eligible resistance to fatigue crack propagation too.

The fatigue crack growth resistance of the investigated base materials is different in different crack path directions, which depends on the material grade too.

The welding causes unfavourable effects both on the mechanical properties and the fatigue crack growth resistance of the high strength steels.

Based on these results and the used methods, fatigue crack propagation limit curves can be determined for the investigated high strength steel base materials and their gas metal arc welded joints.

The selected values of the Paris exponents (n) for the fatigue crack propagation limit curves of the investigated welded joints were higher than the exponents of the concerning base materials, in both mismatch conditions.

Both the mismatch condition and the heat input have significant effects on the fatigue crack growth characteristics on the investigated high strength steel welded joints.

The limit curves on the one hand correctly reflect the fatigue crack growth characteristics of both the base materials and the welded joints, on the other hand are usable for structural integrity and/or reliability assessment calculations.

The research work should be continued. Further examinations and analyses required in order to draw statistically better established conclusions, to measure threshold stress intensity factor range (ΔK_{th}) values for base materials and welded joints, to reveal the influence of the welding technological parameters and finally, to study the effects of the welding residual stress fields.

REFERENCES

[1] Schütz, W. (1996). A history of fatigue. *Engineering Fracture Mechanics*, Vol. 54, No. 2, pp. 263–300, ISSN 0013-7944.

[2] Paris, P. C., Gomez, M. P., Anderson, W. E. (1961). A rational analytic theory of fatigue. *The Trend in Engineering*, Vol. 13, pp. 9–14.

[3] Paris, P., Erdogan, F. (1963). A critical analysis of crack propagation laws. *Journal of Basic Engineering*, Vol. 85, pp. 528–533.

[4] Schroepfer, D., Kannengiesser, T. (2016). Stress build-up in HSLA steel welds due to material behavior. *Journal of Materials Processing Technology*, Vol. 227, pp. 49–58, ISSN 0924-0136.

[5] Lausch, T., Kannengiesser, T., Schmitz-Niederau, M. (2013). Multi-axial load analysis of thick-walled component welds made of 13CrMoV9-10. *Journal of Materials Processing Technology*, Vol. 213, pp. 1234–1240, ISSN 0924-0136.

[6] Schroepfer, D., Kromm, A., Kannengiesser, T. (2015). Improving welding stresses by filler metal and heat control selection in component-related butt joints of high-strength steel. *Welding in the World*, Vol. 59, No. 3, pp. 455–464, ISSN 0043-2288.

[7] Ravi, S., Balasubramanian, V., Nemat Nasser, S. (2004). Effect of mis-match ratio (MMR) on fatigue crack growth behaviour of HSLA steel welds. *Engineering Failure Analysis*, Vol. 11, No. 3, pp. 413–428, June 2004, ISSN 1350-6307.

[8] Mobark, H. F. M., Lukács, J. (2018). Mismatch effect influence on the high cycle fatigue resistance of S690QL type high strength steels. *2nd International Conference on Structural Integrity and Durability*, Dubrovnik, Croatia, October 2–5.

[9] Balogh, A., Lukács, J., Török, I. (eds.) (2015). *Weldability and the Properties of the Welded Joints*. University of Miskolc, Miskolc, p. 324 (In Hungarian), ISBN 9789633580813.

[10] Dobosy, Á. (2017). *Design limit curves for cyclic loaded structural elements made of high strength steels*. PhD Thesis, István Sályi Doctoral School of Mechanical Engineering Sciences, University of Miskolc, Miskolc (In Hungarian).

[11] Gáspár, M. (2016). *Welding technology development of Q+T high strength steels based on physical simulation*. PhD Thesis, István Sályi Doctoral School of Mechanical Engineering Sciences, University of Miskolc, Miskolc, (In Hungarian).

[12] BS 7910:2013+A1:2015: *Guide to methods for assessing the acceptability of flaws in metallic structures*. BSI Standards Limited, 2015.

[13] ASTM E647-15e1: *Standard Test Method for Measurement of Fatigue Crack Growth Rate.* ASTM International, 2015.

[14] Lukács, J. (2003). Fatigue crack propagation limit curves for different metallic and non-metallic materials. *Materials Science Forum*, Vol. 414–415, pp. 31–36, ISSN 1662-9752.

Design of Machines and Structures, Vol. 10, No. 1 (2020), pp. 39–48.
Doi: 10.32972/dms.2020.005

DEVELOPMENT OF AN ELECTRIC MEASUREMENT SYSTEM FOR RAPID DETERMINATION OF THE FRICTION COEFFICIENT

LÁSZLÓ RÓNAI

University of Miskolc, Robert Bosch Department of Mechatronics
3515, Miskolc-Egyetemváros
ronai.laszlo@uni-miskolc.hu

Abstract: Development of an electric measurement system for rapid determination of the friction coefficient is discussed in this paper. The electric system is capable to use with a ball cage guide bush unit. Two beam load cells are included into the system and the measured values of the forces are processed by microcontrollers. In the course of measurements, normal- and tangential forces of inner or outer surfaces of different enamelled specimens could be determined. A data acquisition program is developed to record the force values to a personal computer. Linear interpolation method is required to synchronize the values of the load cells, which is necessary to calculate the coefficient of friction.

Keywords: *friction coefficient, microcontroller, Arduino*

1. INTRODUCTION

The friction as phenomenon can be experienced in everyday life. The behaviour of mechanical systems, which contain moving parts, strongly influenced by the friction [1]. There are several friction models, e.g. Dahl, viscous, Stribeck model, etc., which can be used for different aspects [1], [2]. The most common model is the Coulomb model of friction, which deals with the dry friction. In many problems, this model is adequate to use.

The so-called friction coefficient can be measured experimentally with different methods. The static and kinetic friction coefficients can be calculated with use of an inclined plane [3], [4]. These experimental setups consist a slope and its angle can be varied. Due to the change of the angle, the specimen may begin to tilt on the plane. When the specimen starts to move, the current angle of the inclined plane provides the static friction coefficient. In [5] an experimental setup contains a S-shaped load cell, which used to measure the tensile force of the friction.

The main purpose of the paper is to develop an electrical device for the measurement system, which is capable to use for rapid and approximate determination of the friction coefficient. Mechanical design of the construction is detailed and summarized in [6]. Internal and external surfaces of the measured specimens, e.g., enamelled aerosol cans, have different friction coefficients. The measurement system contains two load cells, three Arduino Nano prototype board with AVR type ATmega328 microcontrollers [7], two A/D converters, and two transmission sensors.

This paper is organized as follows: Section 2 contains the designing aspects of the electrical system and describes the whole device. Section 3 deals with the programs developed for the microcontrollers and for a laptop. Section 4 details the determination of the friction coefficient. A special purpose program is developed to use the linear interpolation method to synchronize the values of the load cells for the same timestamp. A test measurement is also demonstrated. The Section 5 has concluding remarks.

2. DESIGNING OF THE MEASUREMENT SYSTEM

The main function of the machine is to determine rapidly the friction coefficient. The model of the unit is shown in *Figure 1*. A specimen of an aerosol can, which may have different diameters can be fixed to a ball cage guide bush with a hold-down element. The radial surface of a holder is manufactured to a revolver one. Therefore, specimens can be inserted onto the holder with different diameters. Due to revolver shaped holder the friction coefficients of the inner and outer surfaces of the cans can be also measured. A steel tool, which is placed onto the specimen, is kept in a permanent position by a sheet metal in the course of the measurement.

The guide bush is moved with a handle manually. Since the measurement of both normal- and tangential forces are required at the same time to determine the friction coefficient, the system contains two beam shaped load cells. The tangential force is measured by a load cell LC_t and the normal force is determined by another load cell LC_n *(*see *Figure 1)*. A predefined load in normal direction can be adjusted with a winding knob. A ball bearing is in the bottom of LC_n to roll when the guide bush is moved. The capacities of the above-mentioned load cells are different. The maximum allowable forces of LC_t and LC_n are 50 N and 200 N, respectively. The positive velocity of the guide bush is denoted by v+. A spring is added to the threaded shaft to provide a relatively constant normal force during the measurement.

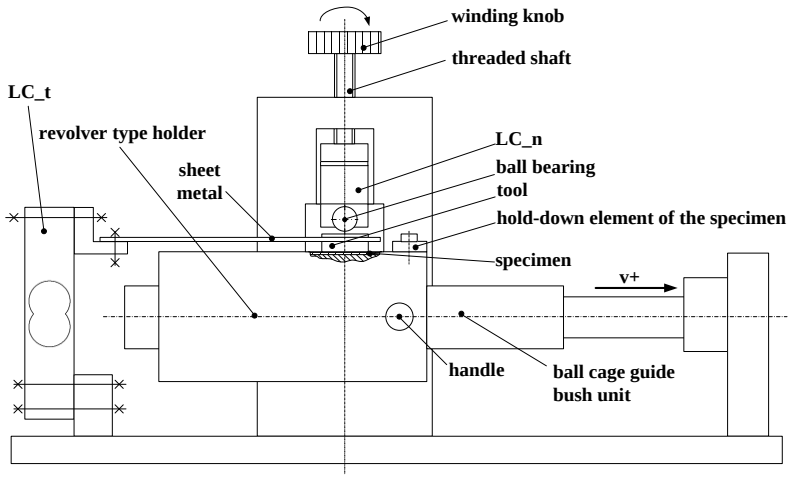

Figure 1. Model of the measurement system

The block scheme of the electrical system is shown in *Figure 2*. A beam load cell contains four strain gauges, which are wired to each other in a Wheatstone bridge configuration. Due to bridge configuration the change of resistance is transformed to change in the bridge voltage. The voltage can be measured by a HX711 type 24-bit sigma-delta A/D converter [8] with 80 Hz sampling rate. The data are sent via serial communication protocol to the microcontrollers MC 1 and MC 2. The forces are determined by a self-devised program. Scaling of incoming data is performed by the program. These values are transmitted to a laptop with UART communication protocol.

Two transmissive sensors are used to calculate the average velocity of the guide bush. These optical sensors have a phototransistor and an infrared emitter in a face-to-face configuration. The elapsed time between the base and end position is measured by a microcontroller MC 3, which provide an average velocity in aware of the distance:

$$\bar{v} = \frac{\Delta x}{\Delta t} = \frac{79\,mm}{\Delta t}. \tag{1}$$

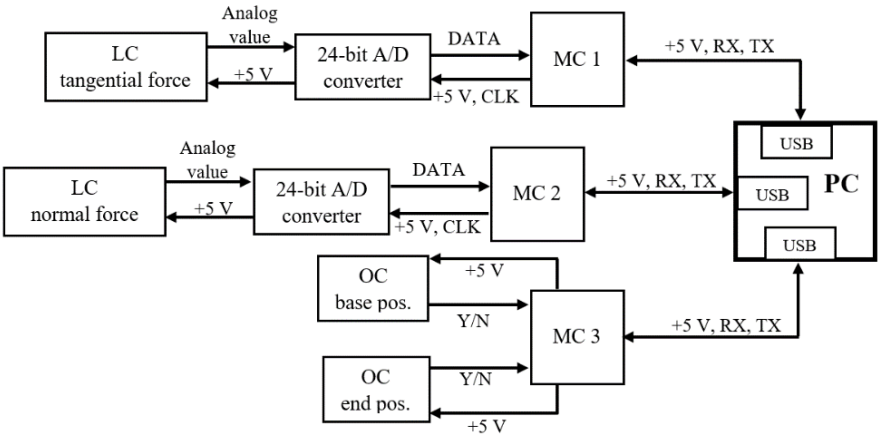

Figure 2. Block scheme of the electric system

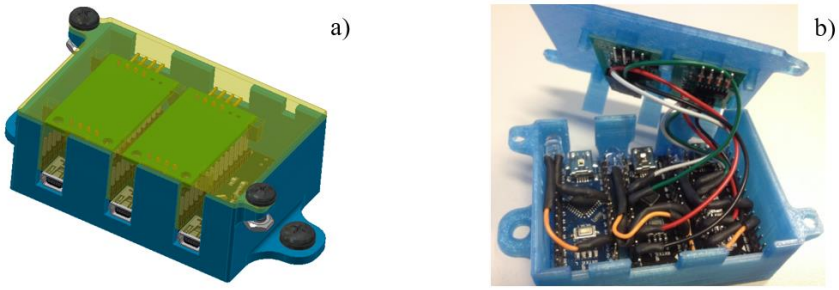

Figure 3. a) 3D modelling of the electric box,
b) Assembling of the electric components

The electric system and its box are designed in Autodesk Inventor software. The box and its cap are manufactured by 3D printing technique using polylactic acid (PLA) filament. Layers are 0.1 mm with rectilinear filling method prescribing 10% infill parameter. The 3D model of the electric box is shown in *Figure 3a* and the manufactured one is given in *Figure 3b*. Three state LEDs with limiting resistors are also built in the box.

The complete measurement system can be seen in *Figure 4*. The electric system is attached to the structure. Cable protection channels are used to prevent the damage of the wires from moving of the handle.

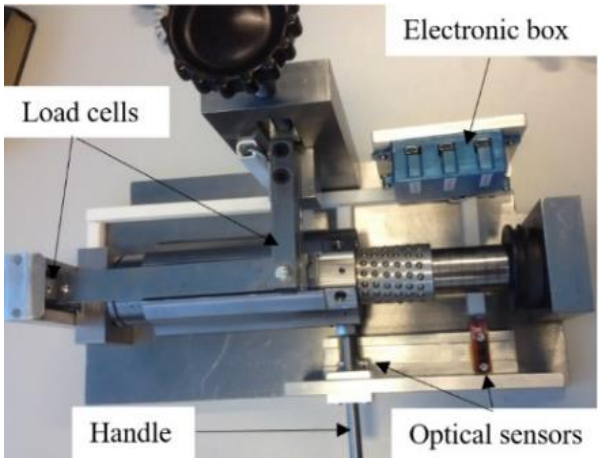

Figure 4. The measurement system

3. PROGRAMS DEVELOPED FOR MICROCONTROLLERS AND LAPTOP

The programs of MC 1–3 are developed in Arduino IDE software in C programming language. The flow chart of the force measurement microcontrollers is shown in *Figure 5*.

Variables and its initial values are defined in the beginning. The pins are initialized at the program part void setup(). The void loop() section is an infinite loop, where MC 1 and MC 2 are reading values from the serial ports connected to a laptop. An if statement is used to carry out a conditional decision based on the incoming characters. If the character is ‘a’ the reading process from the A/D converter is performed and a state LED indicates that the force measurement is active until the incoming character is ‘c’. Before sending the force value to a laptop the float type force values are converted into string of length 10 byte. When the laptop sends character ‘c’, the program jumps to the beginning.

The state LED is inactive when the incoming character is not equal to ‘a’. If the laptop transmits character ‘s’ the microcontroller stores a new base value of the load cell to the onboard EEPROM. The size of the EEPROM is 1 kB. Since the A/D converter has 24 bit resolution therefore, 4 bytes are required to store its raw value.

Two functions have been written for saving and reading raw values. Binary right and left shift operators are used to disassemble and assemble the values of the converter for saving and reading, respectively.

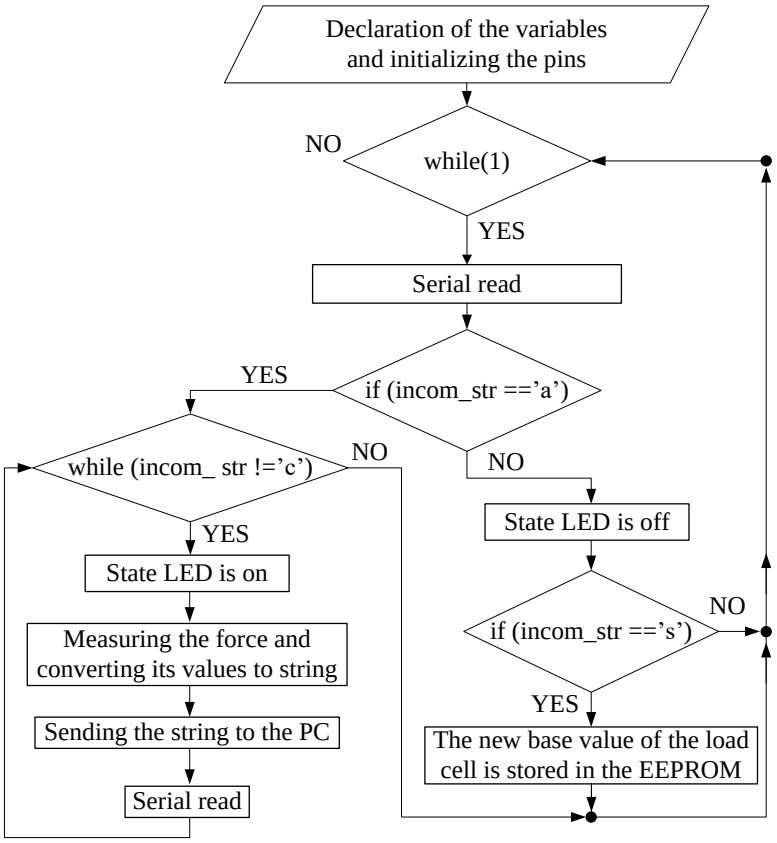

Figure 5. Flow chart of the force measuring microcontrollers

MC 3 measures the elapsed time between the base and the end position of the handle. The flow chart diagram of the MC 3 program can be seen in *Figure 6*. The ATmega328 microcontroller has two external interrupt capabilities.

The definition of the pins and the declaration of the variables and its initial values are belonging to the first step *(*see *Figure 6)*. The initialization of the Interrupt Service Routine (ISR) is the next step. The ISR can be triggered if the logic state of the pin is changed. There are four possibility to initiate an ISR, i.e., LOW, RISING, FALLING, CHANGE modes [9]. When a FALLING mode is chosen the ISR will be executed if the signal has a falling edge from logical 1 to logical 0. The optical sensor of the base position has been attached to D3 pin, which has an ISR capability.

A condition is defined in the void loop() section. If the handle leaves the base position and it arrives to the end position the condition is fulfilled. Thereafter the state LED indicates that the condition is satisfied, and the measured time is sent to the laptop.

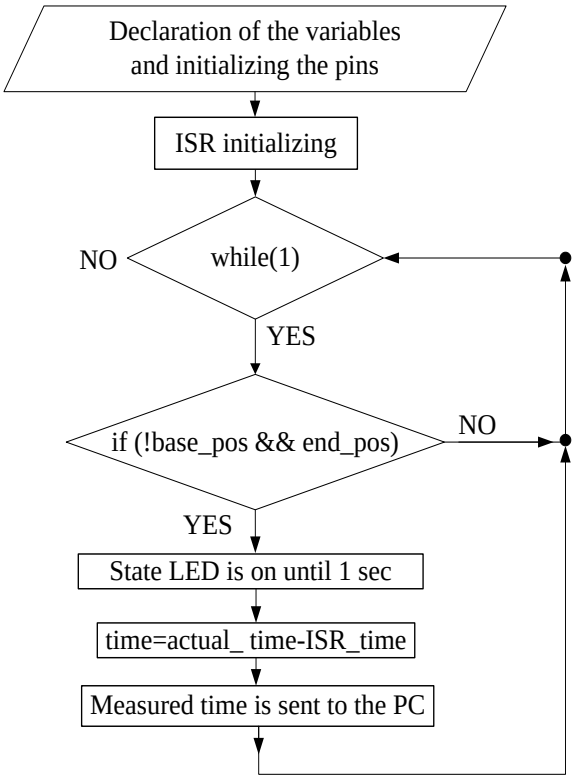

Figure 6. Flow chart of the microcontroller, which measures the elapsed time

A data acquisition program is developed in LabVIEW [10] software. The main frame of the program is created by flat sequence option to ensure a sequence of order in the course of execution. The flow chart of the program can be seen in *Figure 7*. In the first step the variables are initialized. The second step contains a loop with a condition. If the OK button is pressed in the Graphic User Interface (GUI) of the program *(*see *Figure 8)* the zero values of the load cells will be set. When the START button is pressed the program jumps to the third step, where the configuration of the chosen serial ports takes place. The character 'a' is sent to MC 1 and MC 2. The fourth step contains the receiving and displaying section of the incoming data. If the predefined sampling time is over or a STOP button is pressed the program jumps to the fifth step, where the serial ports are closed. The last step of the flat sequence offers a data saving option to store it in .csv file format.

The GUI provides the possibility to prescribe the working serial channels and the sampling time, etc., *(*see *Figure 8)*.

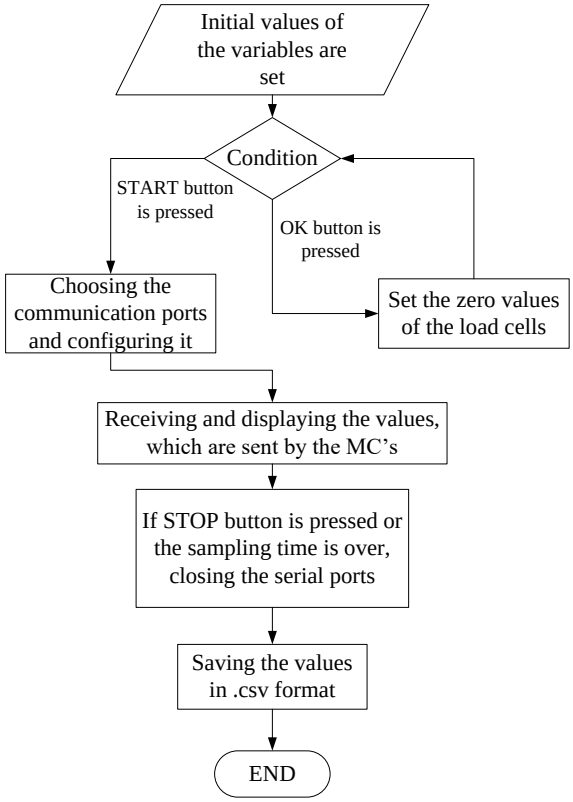

Figure 7. Flow chart of the LabVIEW program

The values of the normal- and tangential forces are displayed with XY Graphs separately. A table is created to store the time and the calculated average velocity of the guide bush.

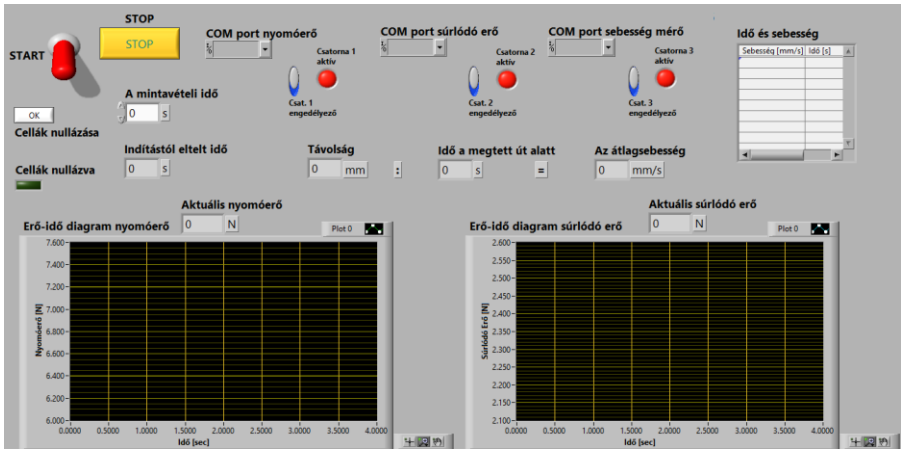

Figure 8. User interface of the program

4. DETERMINATION OF THE FRICTION COEFFICIENT

A special purpose program has been developed in Scilab software [11] to determine the friction coefficient. In order to provide the values of the two load cells in the same time a linear interpolation method [12] is required. Since the A/D converters of the load cells cannot be synchronized, therefore the interpolation can resolve this problem.

The interpretation process is shown in *Figure 9*. In the program the values of the tangential forces are interpolated to the timestamp of the normal forces. The interpolation function *(*see *Table 1)* can be written as follows:

$$S_{interp} = S(i,2) + \frac{[S(i+1,2)-S(i,2)][N(i,1)-S(i,1)]}{S(i+1,1)-S(i,1)}, \tag{2}$$

where $S(i,2)$ is the i^{th} value of the tangential friction force, $S(i+1,2)$ is the $(i+1)^{th}$ tangential force, the time values of these force values are $S(i,1)$, $S(i+1,1)$, respectively. The $N(i,1)$ is the time value, in which the tangential force (S_{interp}) is interpolated.

Table 1

The linear interpolation function in Scilab program system

```
if (N(i,1)>=S(i,1) & N(i,1)<S(i+1,1))
then
   dt=N(i,1)-S(i,1)
   Dt=S(i+1,1)-S(i,1)
   ds=S(i+1,2)-S(i,2)
   S_interp(i,1)=S(i,2)+ds*dt/Dt
   flag=1
end
```

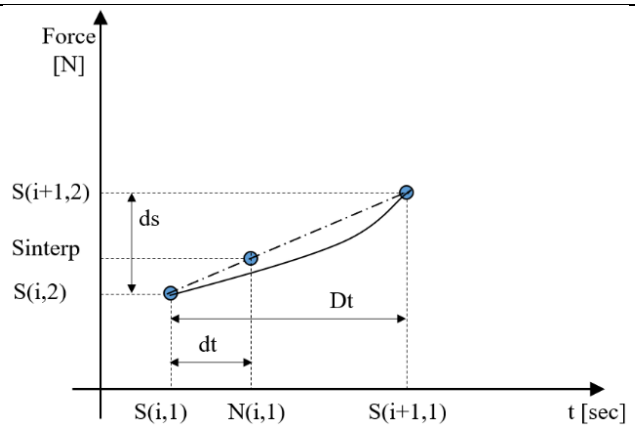

Figure 9. Linear interpolation method

The program reads the raw data in .csv file format. Thereafter the program determines the friction coefficients related to the discrete time values. The friction coefficient μ is obtained by Coulomb friction law

$$\mu = \frac{F_T}{F_N}, \tag{3}$$

where F_T is the tangential force and F_N is the normal counterpart.

Test measurements are performed with different specimens. The result of a test measurement is shown in *Figure 10*, where black solid line represents the measured value, the thin red line its linear regression. The elapsed time of the manually moved handle between the initial and the end position was 0.65 s.

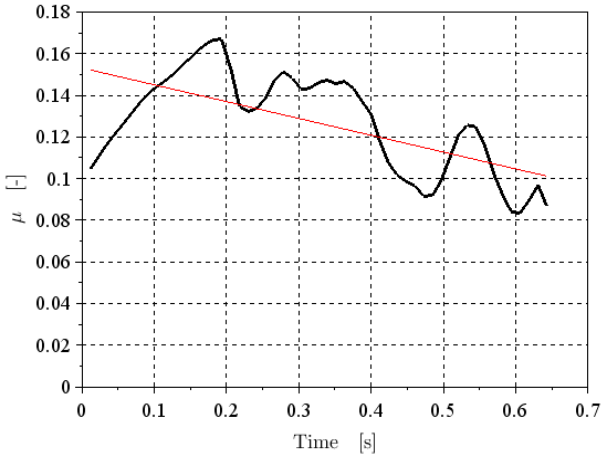

Figure 10. Result of the test measurement

The oscillating result of the friction coefficient μ shows a decreasing tendency, its median value for an aerosol can is approximately 0.125.

The analyzed example demonstrates the effectiveness of the proposed measurement method for rapid testing.

5. SUMMARY

Development of an electric system of a device, which is capable to measure friction coefficient rapidly has been discussed in this paper. The system contains two beam load cells to measure the normal- and the tangential forces. Three microcontrollers are built-in to provide the measured data for a laptop. One of these microcontrollers is used to measure the average velocity of the handle. A box was designed and manufactured with 3D printing technique to protect the electric system. Special purpose programs were developed for the microcontrollers and a data acquisition program was also developed to display and store the force values. A Scilab program was written to postprocess of the measured values in order to determine the median value of the friction coefficient.

The test measurements show that the developed device is well applicable in practice. The friction coefficients of inner or outer surfaces of specimens could be determined.

ACKNOWLEDGEMENT

The described article was carried out as part of the EFOP-3.6.1-16-2016-00011 *Younger and Renewing University – Innovative Knowledge City – institutional development of the University of Miskolc aiming at intelligent specialisation* project implemented in the framework of the Szechenyi 2020 program. The realization of this project is supported by the European Union, co-financed by the European Social Fund.

REFERENCES

[1] Andersson S., Söderberg A., Björklund S. (2007). Friction models for sliding dry, boundary and mixed lubricated contacts. *Elsevier Ltd., Tribology International*, Vol. 40, Issue 4, pp. 580–587.

[2] Liu, Y. F., Zhang, Z. M., Hu, X. H., Zhang, W. J. (2015). Experimental comparison of five friction models on the same test-bed of the micro stick-slip motion system. *Mech. Sci*., 6, pp. 15–28.

[3] Lorestani, A. N., Rabani, H., Khazaei, Y. (2012). Design and construction of an automatic coefficient of friction measuring device. *Agric. Eng. Int.: CIGR Journal*, Vol. 14, No. 1, pp. 120–124.

[4] Aznar Fernández, Juan Diego (2015). *Experimental determination of the friction coefficient using a tilted plane*. pp. 1–5. Doi: 10.13140/RG.2.1.3851.2161.

[5] Hasankhani-Ghavam, F., Abbaspour-Gilandeh, Y., Shahgoli, G., Rahmanzadeh-Bahram, H. (2015). Design, manufacture and evaluation of the new instrument to measure the friction coefficient of soil. *Agric. Eng. Int.: CIGR Journal*, Vol. 17, No. 1, pp. 101–109.

[6] Gál, G. (2019). *Experimental Determination of the Friction Coefficient*. Study, University of Miskolc (in Hungarian).

[7] Atmel (2009). *8-bit AVR Microcontroller with 4/8/16/32K Bytes In-System Programmable Flash*. Datasheet, Rev. 8025I–AVR–02/09.

[8] *AVIA Semiconductor: 24-Bit Analog-to-Digital Converter (ADC) for Weigh Scales.* Datasheet, 2016.

[9] Arduino prototyping platform: https://www.arduino.cc/.

[10] Larsen, R. W. (2011). *LabVIEW for Engineers*. Prentice Hall, Upper Saddle River, New Jersey.

[11] The Scilab Consortium: http://www.scilab.org.

[12] Lepot, M., Aubin, J. B., Clemens, F. H. L. R. (2017). Interpolation in Time Series: An Introductive Overview of Existing Methods. Their Performance Criteria and Uncertainty Assessment. *Journal Water*, Vol. 9, Issue 10, pp.1–20.

Design of Machines and Structures, Vol. 10, No. 1 (2020), pp. 49–62.
Doi: 10.32972/dms.2020.006

EVOLUTIONARY BASED SYSTEM FOR QUALIFICATION AND EVALUATION – A CASE STUDY

FERENC JÁNOS SZABÓ

University of Miskolc, Department of Machine and Product Design
3515, Miskolc-Egyetemváros
machszf@uni-miskolc.hu

Abstract: In a previous paper the new EBSYQ (**E**volutionary **B**ased **SY**stem for **Q**ualification and Evaluation of Group Achievements) system has been proposed for teachers and juries, helping them in making accurate and objective ranking. The analysis of the behaviour of the special characteristic sigmoid functions of the groups gives the possibility to discover some interesting points of view for qualifying the achievement and the standard of the groups (subgroups of talented and under- motivated students, spectrum of the group, eigenvalues, Lorentz function). This paper shows a case study of an international project of student groups competition in the field of product design, with Finnish and Hungarian students. Comparison of the decision process of the jury without using the EBSYQ system and with the application of the system shows the efficiency of the qualification system in realizing a well-founded and careful ranking of the groups, even in case of very close competition. Each point of view of the decision-making system is evaluated by numbers, which can increase the objectivity and accuracy of the decision.

Keywords: *Sigmoid functions; evolutionary based system; evaluation, qualification and comparison of group achievements; EBSYQ methodology of qualification and evaluation.*

1. INTRODUCTION

In this paper a system is shown and applied for evaluation, ranking and comparison of results and achievements of groups or teams. The proposed system for comparison and evaluation (EBSYQ) [1] can provide advantages to each participant in engineering education, testing or competitions: Teachers could more easily find the target groups for special attention (close- up consultations, coaching, special instructions, talent treatment etc.), the jury or decision makers could make decisions or selections more quickly and objectively, eminent students could receive prizes or appropriate ranking based on objective and accurate decisions, failing student could receive more appropriate and targeted special consultations.

The efficiency of the proposed system is demonstrated through a case study of an international project competition (RePCI, **Re**shaped **P**artnerships for **C**ompetitiveness and **I**nnovation Potentials in Mechanical Engineering) of students. The decision-making process of the jury deciding the winning team of the competition is

compared when they make the decision without using the EBSYQ system and we can see the advantages when the system is used.

The case study shows that without the proposed system the results of the groups are extremely close, if in one criterion one group was better, the other group was better from an other point of view, so the final decision would normally contain a high percentage of subjectivity. Since the new system is able to detect and compare numerically every small differences, this subjectivity can be eliminated and the decisions will be more objective, more precise and based on accurate numerical justification.

2. CASE STUDY: INTERNATIONAL STUDENT PROJECT ON PRODUCT DEVELOPMENT

Between September 2014 and January 2015, within the framework of the EU-financed RePCI [2] (**Re**shaped **P**artnerships for **C**ompetitiveness and **I**nnovation Potentials in Mechanical Engineering) international project [3], JAMK (Jyväskylä University of Applied Sciences, Finland) and UM (Institute of Machine and Product Design, University of Miskolc, Hungary) [4] carried out an international student project in product development, titled "Design of a multifunctional garden tool" with the helps and suggestions of the experts of Robert Bosch Power Tool Company, Miskolc, Hungary.

Each partner university participated with an 8-member team, two teams were formed, each with 3 Finnish and 5 Hungarian students. The two groups received the same instructions and the same objective, but after this the groups worked separately, within competition-like circumstances, without communication between the two groups, even keeping their results secret from each other.

The objectives of the project were to:

- Increase intercultural competence
- Solve real-life problems
- Make contacts with international companies
- Gain interdisciplinary project skills
- Obtain deeper knowledge in project management
- Communication between group members during project realisation
- Increase social competence and communication skills
- Improve the ability to work in teams.

The total time of the project was one complete semester and the students worked in the project as if completing a course, receiving 5 credits at the end. Two intensive weeks were organised: the first intensive week was at the very beginning of the project, in September 2014, in Miskolc, Hungary, with an introduction section, and a chance for the Finnish and Hungarian students to get acquainted. During a visit to the Bosch factory, the students received the description of the task, requirements of the product to be designed and all the necessary instructions to start the project. They selected their own team leader from the members of the team, and

they made every decision concerning the necessary steps of the solution, time scheduling, task distribution amongst the team members, etc. Two supervisors (teachers of mechanical engineering, with project realisation experience) visited both teams regularly to answer questions and give useful instructions during the solution of the problems.

After the first intensive week the group members continued their work using communication possibilities offered by the Internet (Google, Skype, e-mail, chat, Facebook etc.). They solved the questions and sub-problems decided and distributed during the first intensive week and they exchanged their results. This system was a great challenge for the team leaders as well, working with groups with members in different countries.

The second intensive week was in Jyväskylä, Finland, at the end of October 2014. After one month of working, during this intensive week they put together their task results, started to form the main concept of the designed product, and determined the further steps necessary to solve the task completely. After the intensive week everyone continued the work, similarly to after the first intensive week.

The project ended with a video-conference day in January 2015, where both groups presented their results, each student having the chance to present his/her own results, ideas and solutions in 5–10 minutes. After the presentations they responded to the questions and comments of supervisors, project manager, or others in the audience. The work of the students was evaluated by the expert of the Bosch factory and by the supervisors. Representatives of the local press (TV, radio, newspapers) reported this event in the news, showing the pictures of the resulting products of the teams, giving a wider platform and reputation to the work and results of the students.

2.1. Comparison of the groups without the EBSYQ system

At the end of the semester, the project reaching the stage of evaluating, comparing and ranking the teams and the students participating in the project. Supervisors and managers of the project and institutions together had to give detailed opinions and evaluations on the work and results of the groups. Since both of the teams worked excellently and each had a new and fully elaborated concept of a garden tool as their result, the jury was really in a difficult position in making the decision of which group could be the winner. As shown in *Table 1*, the two groups were very good and their results were equivalent – if one group was better in one point of view, other group was better in a different aspect. At that time the system proposed in this paper was not yet available, therefore the decision at the end was very subjective: Group A was chosen as the winning team, but the close result and outstanding work of both groups were emphasised. *Table 1* shows the points of view used for the comparison of the groups and the points given (average points given by the members of the jury).

Table 1
Comparison of groups without EBSYQ system
(out of five points per item)

Points of view	Group A	Group B
Communication, interaction, attention to each other	4	5
Distribution of tasks, organisation of the work	3	4
Time scheduling, creating and meeting deadlines	5	3
Partitioning the tasks and assigning them to members	4	4
Forming the main conception of the product	5	4
Price-analysis, material and technology costs	5	4
Taking into account the opinion of the customers	4	5
Marketing, advertising and communicating results	5	4
Presentation :		
Timing, rhythm, fluency	5	4
Content, quality	4	4
Figures, pictures, colors	4	5
Each member presents his/her results	4	5
Communication with supervisors, questions	4	5
Sum of the points	56	56

2.2. Comparison using the EBSYQ system

For comparison, the usage of the evaluation and comparison system EBSYQ is demonstrated, following the method of the system, analysing the curves and characteristics of the groups. Since this system needs the point results of the group members, it is necessary to create points for the individual comparison of the students and it is necessary to give the points. This step is the only subjective one in this system. A short description of the group members, without giving the names or without identifying the individuals:

Group A [5]
A1: boy, Hungarian A2: girl, Hungarian A3: girl, Finnish A4: boy, Hungarian
A5: girl, Finnish A6: boy, Hungarian A7: boy, Hungarian A8: boy, Finnish

Group B [6]
B1: boy, Hungarian B2: girl, Finnish B3: girl, Hungarian B4: boy, Hungarian
B5: boy, Hungarian B6: boy, Hungarian B7: boy, Finnish B8: boy, Finnish

Table 2 gives all the results of the comparison points of view, taking into account separately each group members, possible points are 1 to 5. On the basis of the data given in *Table 2*, it is possible to create the logistic function, the growth function and the first derivative of the logistic function. In order to create the life-curve, it is necessary to „translate" these points into grades (1–5): for this reason, the following limits were created: until 40 points, the mark is 1. From 41 to 45 the mark is 2. From 46 to 50 the mark is 3. From 51 until 55 the mark is 4, and 56 or above is 5. Using these limits, *Table 3* shows how many students obtained a given mark in the groups. (The close competition can be seen here too, because the average of the marks in both groups is the same, 3.62).

Figure 1 shows the resulting curves based on the data of the *Table 2*. The parameters of the approximating logistic curve and growth curve are given in *Table 4*. The approximation curves can be seen in *Figure 2*. It can be observed that the growth curve is very close to the logistic curve, so both can give a good approximation. All the characteristics used for the comparison are collected in *Table 6*. It can be seen in the figures and tables that in the case of Group B, the effect of a possibly under-motivated (low performing) subgroup is weaker than in case of Group A, because the regression coefficient of the logistic function is smaller for Group B. The shape of the result curves, approximation curves and the derivative of the logistic function is very similar for the two groups, also showing the close competition. Minimal slow tendency can be seen in the curves shown by a horizontal part of the curves, but these sections are short, which means that only a few students are included. The value (point result) of the under-motivation zone in Group A is 45, while in of Group B it is 50. The number of students involved: in Group A: 2, in Group B: 4. Note that a second horizontal part with 2 students can be found in Group A around 50 points.

Table 2
Individual points of group member students

Point of view	**A 1**	**A 2**	**A 3**	**A 4**	**A 5**	**A 6**	**A 7**	**A 8**	**B 1**	**B 2**	**B 3**	**B 4**	**B 5**	**B 6**	**B 7**	**B 8**
English language	4	3	3	4	5	4	4	3	4	3	3	4	4	4	3	5
Com-puter skills	4	3	3	5	4	4	5	3	5	4	4	4	5	4	3	5
Engng skills	4	4	4	5	4	5	5	4	5	4	4	5	4	5	4	5

Point of view	A 1	A 2	A 3	A 4	A 5	A 6	A 7	A 8	B 1	B 2	B 3	B 4	B 5	B 6	B 7	B 8
Economy skills	3	4	4	3	5	4	4	3	4	4	3	4	4	3	3	4
Manager skills	3	4	3	4	5	3	4	3	4	3	4	4	5	4	4	5
Communication	4	4	3	4	5	4	5	3	4	4	4	4	5	4	4	5
Intercultural skills	3	3	3	5	5	4	4	3	4	3	4	5	5	4	4	5
Tolerance	4	4	4	5	5	4	4	3	4	3	4	4	5	4	4	4
Integration	5	4	3	5	5	4	5	3	5	3	4	4	5	4	4	5
Commun. with superv	4	4	3	5	5	4	4	3	5	3	4	4	4	5	4	5
Presentation	5	5	4	5	5	4	5	4	5	3	4	4	5	5	4	5
Quality of results	4	4	4	5	5	4	5	3	5	3	4	4	5	4	4	5
Teammember skills	4	4	3	4	5	4	4	3	4	3	4	4	5	5	4	4
Sum of points	51	45	44	59	63	52	58	41	58	43	50	54	49	55	49	62

Table 3
Data for the life curves of the groups

Group	points	41–45	46–50	51–55	56–65
A	Grade	2	3	4	5
	No. of students	3	0	2	3
B	Grade	2	3	4	5
	No. of students	1	3	2	2

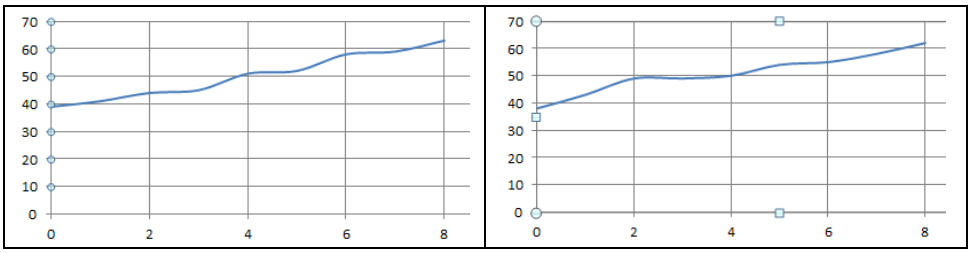

Group A Group B

Figure 1. Result curves of the groups, on the basis of individual points

Table 4
Parameters of the approximation curves

curve type	**Group A**				**Group B**			
	K	*r*	*c*	Regr. coef.	*K*	*r*	*c*	Regr. coef.
logistic	64	0.35	1	–0.922	62.5	0.36	0.71	–0.878
growth	64	0.24	0.5	–0.896	62.5	0.25	0.4	–0.848

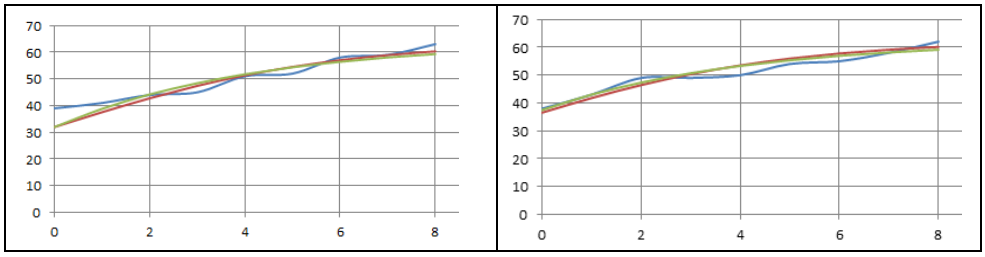

Group A Group B

Figure 2. Approximation curves of the groups. The growth curve is very close to the logistic curve.

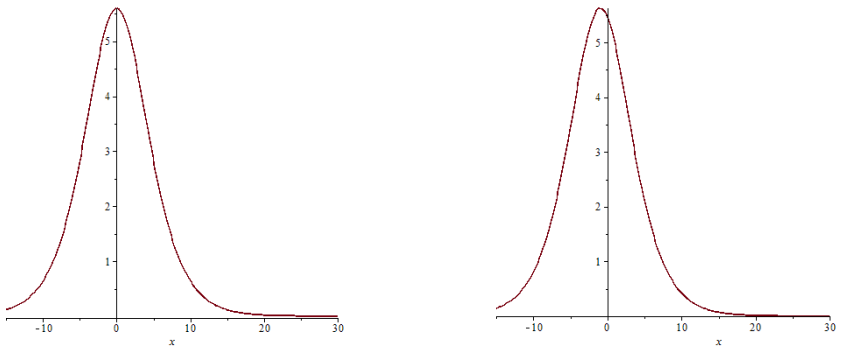

Group A Group B

Figure 3. First derivative of the logistic curves of the groups

A part of the curve showing better than average motivation can be seen in the curve of Group B from 40 to 50 points, and for Group A this is from 35 to 45, so a slightly smaller. Another good motivation section can be found for Group A at 58 points (2 students) and for Group B around 50 points, with 3 students. Table 6 shows several points of view which gives equal points for the groups. This phenomenon decreases the number of the available points, so instead of a maximum of 32 points in this case there will be only 26.

The maximum of the growth velocity is somewhat higher for Group B (5.7) than for Group A (5.5), but the place of the maximum is around 0 or in the negative zone, therefore, this maximum is only theoretical, it does not show the effect of a subgroup. The best point result in Group A is 63 and in Group B it is 62.

Table 5
Data necessary for Lorentzian curves of the eigenvalues

		Eigenvalue 1	**Eigenvalue 2**
Group A	*K*	3	3.2
	r	2	5.1
	c	3.02	0.67
Group B	*K*	3	2
	r	3.1	5
	c	0.9	4.9

Analysis of the life-curves and eigenvalues *(Figure 4)* also shows the similarity of the groups and the close competition: each group has two eigenvalues. The data necessary to write the equations of the Lorentzian curves of the groups for all the eigenvalues are collected in *Table 5*. Some differences can be found only in the significance of the eigenvalues and in the half-maximum – width. The smaller dispersion height or smaller dispersion width of a group *(Figure 6)* can be explained by the better "cohesion" or by the closer cooperation of the group members. *Figure 5* shows the error functions for the first eigenvalue of the groups.

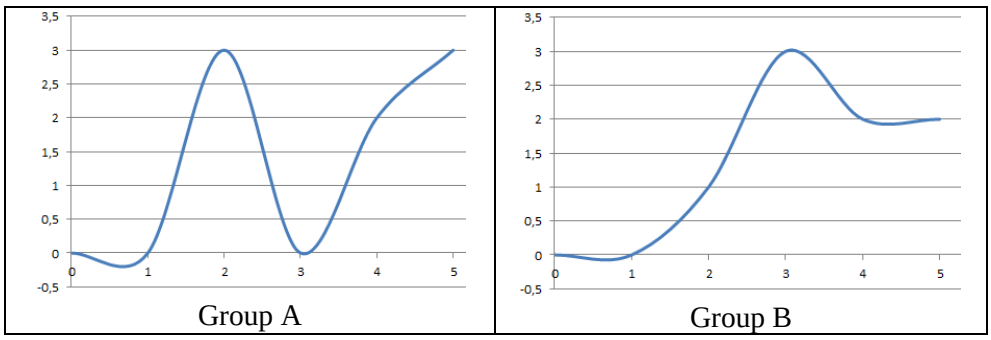

Figure 4. Life curve of the groups

Finally, from the possible 26 points of *Table 6*, Group A wins 14 and Group B wins 12, so the decision is that Group A will be the winner, with 53.85% of the points while Group B has 46.15% of the points. (soccer-like result: 7 to 6 for Group A, it was really a very close fight!).

Table 6
Summarizing table of the characteristics

Type of curve	**Parameter name**	**Notation**	**Group A**	**Group B**	**Comment**	**Wins**
Real curve of results	Slow growth (horizontal)	L/H	0.04	0.076	Length/value	A
	No. of students involved	n	3	4	More motivation needed	A
	Average of point results	P_{av}	3.62	3.62	Easily comparable	–
Growth function	Regression coefficient	R_{kg}	–0.896	–0.848	Strength of correlation	A
	K	*K*	64	62.5	Capacity of the group	A
	r	*r*	0.24	0.25	Evolution (growth) velocity	B
	c	*c*	0.5	0.4	Parameter with mixed effect	–
Logistic function	Regression coefficient	R_{kl}	–0.922	–0.877	Strength of conclusions	B
	No. of failed students	A_m	2	0	Undermotivation	B
	K	*K*	64	62.5	Capacity of the group	A
	r	*r*	0.35	0.36	Growth speed	B
	c	*c*	1	0.71	Parameter with mixed effect	–
	Place of under-motivation	M_h	45	50	Point result	B
	No. low motiv. students	M_{sz}	2	4	Sub-group	A
	Excellent value	U	63	62	Record, best result	A
	No. of excellent students	U_{sz}	1	1	Better in the group	–
	Place of higher motivation	E_m	58	50	For which result	A
	No. high motiv. students	E_{sz}	2	3	How many students	B

Type of curve	**Parameter name**	**Notation**	**Group A**	**Group B**	**Comment**	**Wins**
1st deriv. of logist. f.	Maximum growth speed	v_{fmax}	5.5	5.7	High motivation	B
	Place of maximum	v_m	0	–2	For which result	A
Life curve (Lorentz function)	*K*	*K*	3.2	3	At most signif. eigenv.	A
	r	*r*	5.1	3.1	Place and spreading	–
	c	*c*	0.67	0.9	Param. with mixed effect	–
	How many eigenvalues	S	2	2	How many sub-groups	–
	Eigenvalue 1	s_1	2	3	Eigenresult of subgroup 1	B
	Eigenvalue 2	s_2	5	5	Eigenresult of subgroup 2	–
	Eigenvalue 3	s_3	–	–	Eigenresult of subgroup 3	–
	Significance of s_1	Sz_1	3.6	18	Signif. of the expectable result	B
	Signif. of eigenvalue s_2	Sz_2	40.8	10	Signif. of eigenresult	A
	Signif. of eigenvalue s_3	Sz_3	–	–	Signif. of the result	–
	Width at half max. s_1	η_1	0.6	2	Spreading around the result	B
	Width at half max. s_2	η_2	2.5	1	Spreading around the result	A
	Width at half max. s_3	η_3	–	–	Spreading around the result	–
1st deriv. of Lorentz f.	Width of Lorentz profile	b_d	2	5	Dispersion width	A
	Height of Lorentz profile	h_d	16	5	Dispersion height	B
Integral of Lorentz-function	*K*	K_1	0.8803	0.858	No. of students for a result	B
	$r = r_1 / c$	r_1	6.04	3.1	Mixed effect	A
	c	*c*	3.02	0.9	Parameter with mixed effect	–

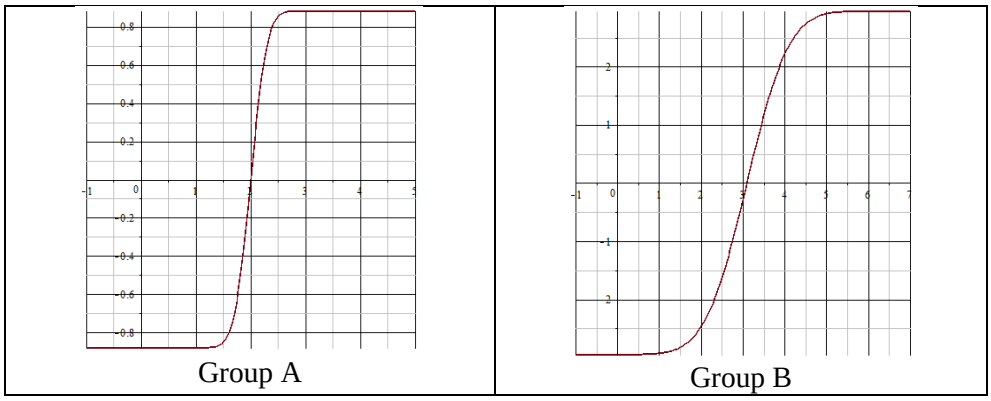

Figure 5. Error functions of the groups
(since K is smaller, Group B wins this point)

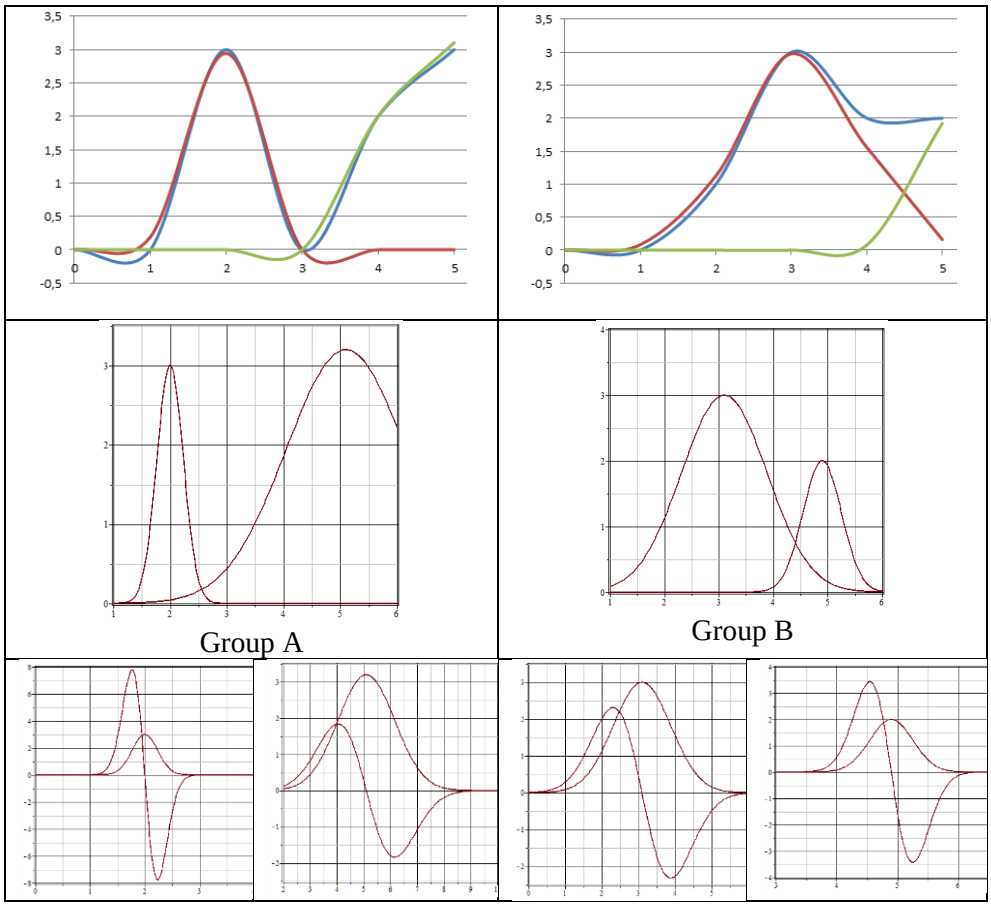

Figure 6. Life curve, eigenvalues and Lorentz profiles of the groups

Equations of the characteristic curves:

Logistic function:	Growth function:	Lorentz function:
$y(x) = \frac{K}{1+ce^{-rx}}$	$y(x) = K(1 - ce^{-rx})$	$y(x) = \frac{K}{e^{c^2(x-r)^2}}$

The Lorentz profile is the first derivative of the Lorentz function.

3. SUMMARY

In this paper an evolutionary based evaluation and qualification system (EBSYQ) is proposed and applied for the comparison of group or team results or achievements. The evolutionary basis of the system comes from the application of sigmoid curves (growth curve, logistic curve), since these curves can be used also for the description of the iteration history of evolutionary type optimisation algorithms. Thirty-eight different points of view are collected for the comparison of the group results, (twelve of these points of view were equal or impossible to decide the winner of it). On the basis of these comparison criteria it will be very easy for a teacher to find the appropriate target–sub-group for a given type of special work or consultation activity (for talented students, competitions for outstanding students, increasing the interest and attendance of average students, or special consultations or remedial work for undermotivated or failed students). The application of this system during a competition among groups (or selection of possible applicants for a job, etc.) makes possible to the decision makers to see the existing differences more clearly, even if they are small, and hard to detect or notice in other ways. This could help a jury or decision makers to make decisions in more objective and accurate manner, numerically evaluating and comparing each point of view during the comparison process. The working and efficiency of the proposed system is shown by the comparison of the decision making process during an international product design cooperation project with the participation of Finnish and Hungarian student groups as a case study, with and without the proposed system. The case study shows that without the proposed system the results of the groups are extremely close, if in one criterion one group was better, the other group was better from an other point of view, so the final decision would normally contain a high percentage of subjectivity. Analysis of the case study by the EBSYQ system proves that the proposed method can detect and separate even very small differences clearly and characterise them numerically, which can be useful help even in case of very close competitions.

Application of the EBSYQ evaluation system of group achievements can be an efficient tool in several decision-making situations in scientific and education fields, resulting more accurate and more objective decisions, which can give advantages to teachers in finding more precisely the target groups for special treatments and consultations, or to decision makers in making better decisions more easily and quickly, to the students or to the members of evaluated groups to win and obtain with higher probability and on more objective basis the prize they are compete for and to arrive more surely in a position where they can enjoy the results of their long, hard and

diligent work. These results can be also useful during increasing the development and methodology skills [7] of students and designers, as well as during the design of talent- treatment, talent- nurturing programmes [8].

Further research in this theme could be to extend this system to other fields of life: analysis and comparison of sports results (groups, individuals) or analysis of evolutionary type optimisation algorithms.

ACKNOWLEDGEMENTS

In connection with the case study shown in this paper, the authors would like to say special thanks to the project RePCI (**Re**shaped **P**artnerships for **C**ompetitiveness and **I**nnovation Potentials in Mechanical Engineering), co-financed by EU Lifelong Learning Program. The research work presented in this paper is partly based on the results achieved within the following project:
HEIBus 575660-EPP-1-2016-1-FI-EPPKA2-KA (Smart HEI- Business Collaboration for Skills and Competitiveness) ERASMUS+ International Project
(HEI = Higher Education Institutes).
The realization of this project is co-supported by the European Union, co-financed by the European Social Fund.

REFERENCES

[1] Szabó, F. J. (2017). Evolutionary Based System for Qualification and Evaluation of Group Achievements (EBSYQ). *International Journal of Current Research*, Vol. 9, Issue 08, pp. 55507–55516, ISSN: 0975-833X, www.journalcra.com/sites/default/files/21246.pdf

[2] Kakko, A. (2016). Reshaped Partnerships for Competitiveness and Innovation Potentials in Mechanical Engineering (RePCI). *44th SEFI (European Society of Engineering Education) Conference*, Tampere, Finland.

[3] Firescu, V., Lapusan,C., Mandru, D., Aksovaara, S. (2015). New Approaches to Increase Organisational Competitiveness Using Competence Coaching Concept. *Review of Management and Economic Engineering*, Vol. 14, No. 2, pp. 273-278, http://www.mee.org/56engleza.htm

[4] Bognár, G. (2015). Reshaped Partnership and Good Practice in Engineering Education. *18th International Conference on Interactive Collaborative Learning (ICL), IEEE Conference Publications*, Florence, Italy. pp. 957–963, doi: 10.1109/ICL.2015.7318157.

[5] Birta, T., Herbst, D., Kiss, G., Kivihalme, K., Kublik, B., Mezei, M., Oinonen, K., Parkkonen, P. (2015). Morphy – the Multifinctional Cordless Garden tool. (Product Design Project). *Design of Machines and Structures*, Vol. 5, No.1. pp. 5–14.

[6] Nagy, G., Spisák, B., Szója, A., Szántai, I., Jalkanen, J., Mattila, J., Rentola, M., Puskás, T. (2015). Branch Shaker Designing Project. *Design of Machines and Structures*, Vol. 5, No. 2, pp. 17–29.

[7] Kamondi, L., Sarka, F., Takács, Á. (2011). *Fejlesztés-módszertani ismeretek* [Development-Methodology Skills] (in Hungarian). Electronic textbook for students, TÁMOP-4.1.2-08/1/a-2009-0001, Miskolc.

[8] Bérczes, R. (2015). The Improvement of Higher Education Quality and Talent-nurturing with Scientific Students' Association (SSA) Commitment. *Acta Polytechnica Hungarica*, Vol. 12, No. 5, pp. 101–120.

REVIEWING COMMITTEE

Secreteriat of the Vice-Rector for Research and International Relations,
University of Miskolc,
Responsible for the Publication: Prof. dr. Tamás Kékesi
Published by the Miskolc University Press under leadership of Attila Szendi
Responsible for duplication: Erzsébet Pásztor
Editor: Dr. Ágnes Takács
Technical editor, proofreader: Csilla Gramantik
Number of copies printed: 50
Put the Press in 2020
Number of permission: TNRT–2020– 100 –ME
HU ISSN 1785-6892 in print
HU ISSN 2064-7522 online